Molecular Pharmacology Fast Forward. Published on August 4, 2021 as DOI: 10.1124/molpharm.121.000304
This article has not been copyedited and formatted. The final version may differ from this version.

ADP ribosylation factor 6 promotes contraction and proliferation, suppresses apoptosis and is specifically inhibited by NAV2729 in prostate stromal cells

Ruixiao Wang [1], Stephanie Schneider [2], Oliver T. Keppler [2], Bingsheng Li [1], Beata Rutz [1], Anna Ciotkowska [1], Christian G. Stief [1], Martin Hennenberg [1]

[1] Department of Urology, University Hospital Munich, LMU Munich, Munich, Germany; [2] Max von Pettenkofer Institute and Gene Center, Virology, National Reference Center for Retroviruses, Faculty of Medicine, LMU Munich, Munich, Germany

Molecular Pharmacology Fast Forward. Published on August 4, 2021 as DOI: 10.1124/molpharm.121.000304
This article has not been copyedited and formatted. The final version may differ from this version.

Running title: ARF6 promotes contraction and growth of prostate stromal cells

Corresponding author:

Prof. Dr. Martin Hennenberg

Urologische Klinik und Poliklinik, Marchioninistr. 15, 81377 München, Germany

Tel.: ++49-(0)89-4400-74868

Email: martin.hennenberg@med.uni-muenchen.de

Orcid: 0000-0003-1305-6727

Number of text pages: 31

Number of tables: 0

Number of figures: 7

Number of references: 52

Number of words in abstract: 250

Number of words in introduction: 649

Number of words in discussion: 2121

Nonstandard abbreviations:

7-AAD, 7-Aminoactinomycin D; APC, allophycocyanin; ARF, ADP ribosylation factor; BPH, benign prostatic hyperplasia; CCK, cell counting kit; Ct, number of cycles; DAPI, 4′,6-diamidino-2-phenylindole; DMEM, Dulbecco's modified Eagle's medium; EdU, 5-ethynyl-2'-

Molecular Pharmacology Fast Forward. Published on August 4, 2021 as DOI: 10.1124/molpharm.121.000304
This article has not been copyedited and formatted. The final version may differ from this version.

deoxyuridine; FBS, fetal bovine serum; FCS, fetal calf serum; FITC, fluoresceine isothiocyanate; GAPDH, glyceraldehyde 3-phosphate dehydrogenase; gRNA, guide RNA; LUTS, lower urinary tract symptoms; RT-PCR, real time polymerase chain reaction; 5-TAMRA, 5-carboxytetramethylrhodamine

Key words:

ARF6; NAV2729; benign prostatic hyperplasia (BPH); smooth muscle contraction; lower urinary tract symptoms (LUTS)

Molecular Pharmacology Fast Forward. Published on August 4, 2021 as DOI: 10.1124/molpharm.121.000304
This article has not been copyedited and formatted. The final version may differ from this version.

Abstract

The presumed ARF6 inhibitor NAV2729 inhibits human prostate smooth muscle contraction and proliferation of stromal cells, which are driving factors of voiding symptoms in benign prostatic hyperplasia (BPH). However, its specificity and a confirmed role of ARF6 for smooth muscle contraction are still pending. Here, we generated monoclonal ARF6 knockouts in human prostate stromal cells (WPMY-1), and characterized phenotypes of contractility, growth-related functions, and susceptibility to NAV2729 in knockout and control clones. ARF6 knockout was verified by Western blot. Knockout clones showed impaired contraction and actin organization, reduced proliferation and viability, and increased apoptosis and cell death. In ARF6-expressing control clones, NAV2729 (5 µM) strongly inhibited contraction (67% inhibition accross all three control clones), actin organization (72%), proliferation (97%) and viability (up to 82%), and increased apoptosis (5-fold) and cell death (6-fold). In ARF6 knockouts, effects of NAV2729 (5 µM) were widely reduced, including lacking or minor effects on contractions (0% inhibition accross all three knockout clones), actin (18%) and proliferation (13%), and lacking increases of apoptosis and cell death. Viability was reduced by NAV2729 with an IC_{50} of 3.3 µM across all three ARF6 control clones, but of 4.5-8.2 µM in ARF6 knockouts. In conclusion, ARF6 promotes prostate smooth muscle contraction and proliferation of stromal cells. Both are inhibited by NAV2729, which showed high specificity for ARF6 up to 5 µM and represents an attractive compound in the context of BPH. Considering the relevance of smooth muscle-based diseases, shared roles of ARF6 in other smooth muscle types merit further investigation.

Molecular Pharmacology Fast Forward. Published on August 4, 2021 as DOI: 10.1124/molpharm.121.000304
This article has not been copyedited and formatted. The final version may differ from this version.

Significance statement

By knockout of ARF6 in prostate stromal cells, we demonstrate an involvement of ARF6 in promotion of prostate smooth muscle contraction and stromal growth, and define concentration ranges for their ARF6-specific inhibition by NAV2729. Besides the context of benign prostatic hyperplasia and lower urinary tract symptoms, analog ARF6 functions in contraction and growth appear possible in other smooth muscle-rich organs, which merits further attention considering the high clinical relevance of smooth muscle-based diseases.

Molecular Pharmacology Fast Forward. Published on August 4, 2021 as DOI: 10.1124/molpharm.121.000304
This article has not been copyedited and formatted. The final version may differ from this version.

Introduction

ADP ribosylation factor 6 (ARF6) belongs to the superfamily of monomeric GTPases. Major functions of ARF6 include cytoskeletal organization and actin remodeling, roles in endocytosis and vesicular trafficking, cell adhesion, and completion of mitotic cytokinesis in different cell types (D'Souza-Schorey and Chavrier, 2006; Donaldson, 2002; Hongu and Kanaho, 2014; Humphreys et al., 2013; Klein et al., 2006; Luton, 2005; Schafer et al., 2000; Schweitzer and D'Souza-Schorey, 2005). Accordingly, it promotes processes based on actin assembly and cytoskeletal organization, including migration, branching and outgrowth in neuronal cells, filopodia extension, platelet-mediated clot formation and thrombosis, or tumor angiogenesis and metastasis (Charles et al., 2016; Choi et al., 2005; Gauthier-Campbell et al., 2004; Hiroi et al., 2006; Hongu et al., 2016; Miura et al., 2016; Torii et al., 2010; Urban et al., 2016). With NAV2729, a small molecule inhibitor with presumed specificity for ARF6 is available (Yamauchi et al., 2017; Yoo et al., 2016). Recently, inhibition of prostate smooth muscle contraction, and of proliferation of prostate stromal cells by NAV2729 have been reported (Yu et al., 2019). ARF6-mediated promotion of smooth muscle contraction and proliferation appears in fact plausible, considering that both processes are actin-dependent (Hennenberg et al., 2014; Jones et al., 2019; Puetz et al., 2009). However, the specificity of NAV2729 has been rarely examined, and a possible role of ARF6 in smooth muscle contraction or the involvement of ARF6 in NAV2729-mediated effects in prostate cells have not yet been confirmed using knockout models.

Previously reported effects of NAV2729 on prostate smooth muscle contraction and growth of stromal cells were discussed in the context of lower urinary tract symptoms (LUTS) suggestive of benign prostatic hyperplasia (BPH). In BPH, increased prostate smooth muscle tone and prostate growth may cause urethral obstruction, resulting in impairments of urinary

Molecular Pharmacology Fast Forward. Published on August 4, 2021 as DOI: 10.1124/molpharm.121.000304
This article has not been copyedited and formatted. The final version may differ from this version.

flow and bladder emptying, and finally in BPH-related voiding symptoms (Hennenberg et al., 2014; Oelke et al., 2013). Options for medical treatment include α_1-adrenoceptor antagonists, the phosphodiesterase-5 inhibitor tadalafil and 5α-reductase inhibitors, which may improve symptoms, or prevent progression of BPH and reduce the risk for complications and surgery (Oelke et al., 2013). Proposed mechanisms include prostate smooth muscle relaxation by α_1-adrenoceptor antagonists and tadalafil, as well as inhibition of prostate growth by 5α-reductase inhibitors (Oelke et al., 2013). Considering that their overall efficacy is insufficient, together with the high and age-dependent prevalence of LUTS suggestive of BPH and the demographic transition, alternative options for medical treatment are of high demand, requiring identification of new targets and novel candidate compounds. Currently, separate medications are needed to target prostate smooth muscle contraction and growth., Connections between both processes have been merely considered in the past, although both may contribute to LUTS suggestive of BPH.

Consequently, identifying molecular mechanisms linking smooth muscle contraction with stromal growth in the prostate provides new concepts in understanding of BPH, and may offer attractive targets for putative medical interventions against BPH in the future (Hennenberg et al., 2014). Findings obtained by application of NAV2729 to prostate tissues allow to assume such a dual role of ARF6 in proliferation and contraction of prostate smooth muscle cells, which needs, however, to be confirmed (Yu et al., 2019). A similar function has been attributed to the momomeric GTPase RhoA. RhoA-mediated contraction and proliferation of smooth muscle cells has been confirmed for all types of smooth muscle and is widely accepted (Somlyo and Somlyo, 2003). Similar roles of other monomeric GTPases in smooth muscle contraction of different smooth muscle-rich organs are an emerging field (Li et al., 2020a). Considering that widespread diseases including arterial hypertension or obstructive airway diseases are related to abberrant smooth muscle contraction, proving a

Molecular Pharmacology Fast Forward. Published on August 4, 2021 as DOI: 10.1124/molpharm.121.000304
This article has not been copyedited and formatted. The final version may differ from this version.

role of ARF6 in smooth muscle contraction may be of interest even beyond BPH and LUTS. Here, we created ARF6 knockout clones of human prostate stromal cells, to a) confirm a role of ARF6 in smooth muscle contraction and proliferation, and b) to characterize the specificity of NAV2729.

Molecular Pharmacology Fast Forward. Published on August 4, 2021 as DOI: 10.1124/molpharm.121.000304
This article has not been copyedited and formatted. The final version may differ from this version.

Materials and methods

Cell culture

WPMY-1 cells are a SV40 large-T antigen-immortalized cell line, obtained from the stroma of a human prostate without prostate cancer (Webber et al., 1999). It is reported that this cell line is hyperdiploid, X–Y, with chromosome numbers varying from 58 to 68 (Webber et al., 1999). According to the typical composition of the prostate stroma, where smooth muscle cells are the predominant cell type, WPMY-1 cells show characteristics of myofibroblasts and prostate smooth muscle cells, including expression of vimentin, α-smooth muscle actin (α-SMA), calponin and α_{1A}-adrenoceptors, but lacking expression of cytokeratins and tyrosine hydroxylase (Wang et al., 2016; Wang et al., 2015; Webber et al., 1999). Here, polyclonal, parental WPMY-1 cells were used to create ARF6 knockout clones and corresponding controls with ARF6 expression. WPMY-1 cells were purchased from the American Type Culture Collection (ATCC; Manassas, VA, USA), and cultured in RPMI 1640 (Gibco, Carlsbad, CA, USA) supplemented with 10 % fetal calf serum (FCS) and 1 % penicillin/streptomycin at 37 °C with 5 % CO_2. Before addition of NAV2729 or dimethylsulfoxid (DMSO, solvent for NAV2729) to parental WPMY-1 cells, ARF6 knockout clones, or ARF6 control clones, the medium was changed to a FCS-free medium.

Vectors and transfection

pLKO.1 CMV gRNA ARF6 GFP mammalian expression plasmid that contains gRNA for knockout generation in ARF6 gene, and pRZ BFP T2A Cas9 mammalian expression plasmid

Molecular Pharmacology Fast Forward. Published on August 4, 2021 as DOI: 10.1124/molpharm.121.000304
This article has not been copyedited and formatted. The final version may differ from this version.

that contains Cas9 for knockout generation were kindly provided by Veit Hornung, Gene Center, LMU Munich, Germany. The target site for ARF6 gRNA in the ARF6 gene was 5'-TGGGAATGGTGGTCACCGACTGG-3'. The two plasmids were co-transfected (1:1 ratio) into WPMY-1 cells using Human Prostate Stromal Cell (PrSC) Avalanche™ transfection reagent (EZ Biosystems, College Park, MD, USA). For transfection, WPMY-1 cells were plated into 6-well plates, grown to 70 % confluency, and cultured without antibiotics 24 h prior to transfection. Transfection mix for each well contained the two plasmids (4 µg of each plasmid) and 5 µl transfection reagent in 200 µl of Opti-MEM (Gibco), which were merged and incubated at room temperature 15 min before addition to wells. Following dropwise addition of the transfection mixture into wells, plates were centrifuged (300 g, 5 min) and subsequently incubated for 5 h (37 °C, 5 % CO_2), before the medium was replaced by normal, antibiotic-containing RPMI. Successful transfections of plasmids were visually verified under a fluorescent microscope using channels for fluoresceine isothiocyanate (FITC) and 4′,6-diamidino-2-phenylindole (DAPI). Subsequenly, successfully double-transfected cells were separated and isolated by cell sorting, using a BD FACSMelody™ Cell Sorter (BD Biosciences, San Jose, CA, USA) at the Flow Cytometry Facility, Gene Center, LMU Munich, Germany.

Single cell dilution and sequencing

Following cell sorting, cells were diluted in RPMI medium to obtain a final dilution between 0.5 and 1 cell/well. Resulting aliquots were seeded into 96-well plates (100 µl/well), and cultured for 4 weeks (37 °C, 5 % CO_2). Successfully growing clones were sequenced using a MiSeq benchtop sequencing system (Illumina, San Diego, CA, USA) (Schmid-Burgk et al., 2014). After sequencing, following clones were selected for further experiments: three ARF6 knockout clones (monoclonal, heterogenous ARF6 knockout clones), in which three alleles

Molecular Pharmacology Fast Forward. Published on August 4, 2021 as DOI: 10.1124/molpharm.121.000304
This article has not been copyedited and formatted. The final version may differ from this version.

were detected via deep sequencing and 1 out of 3 alleles (referred to as knockout clone C4) or 2 out of 3 alleles (knockout clones B4 and B9) showed an out-of-frame mutation at the site of editing, and three ARF6 control clones. Monoclonal ARF6 control clones went through the whole procedure as the knockout clones but do not show any edited sequence in the region where the gRNA for ARF6 was binding (referred to as control clones A3, C6 and D7). ARF6 knockout and control clones were verified by Western blot, as described below.

Western blot analysis

Cells were prepared in T75 flasks, and protein isolation was performed when cells reached 80 % confluency. For protein isolation, cells were washed twice with ice-cold phosphate-buffered saline (PBS). Subsequently, 600 µl of radioimmunoprecipitation assay (RIPA) buffer (Sigma-Aldrich, Munich, Germany) containing 5 µl protease inhibitor cocktail (P8340, Sigma-Aldrich) were added to each flask. After incubation on ice for 25 min, lysed cells were removed from flasks, and cell debris was removed by centrifugation (10,000 g, 10 min, 4 °C). Protein concentrations were determined using aliquots of 40 µl of each sample and a protein quantification assay (catalog number 740967, Macherey-Nagel, Düren, Germany) according to the manufacturer's instructions. Remaining samples were boiled for 10 min with sodium dodecyl sulfate (SDS) sample buffer (Roth, Karlsruhe, Germany). Samples were subjected to SDS polyacrylamide gel electrophoresis (20 µg/lane), and proteins were blotted on Protran® nitrocellulose membranes (Schleicher & Schuell, Dassel, Germany). For blockage of unspecific binding sites, membranes were blocked with PBS containing 5 % milk powder (Roth, Karlsruhe, Germany) over night. Subsequently, membranes were washed three times (each time for 5 min) with PBS containing 0.1 % Tween 20 (PBS-T), followed by incubation with mouse monoclonal anti ARF6 (sc-7971) antibody or mouse monoclonal anti β-actin antibody (sc-47778) (all from Santa Cruz Biotechnology, Santa Cruz, CA, USA) for 90 min.

Molecular Pharmacology Fast Forward. Published on August 4, 2021 as DOI: 10.1124/molpharm.121.000304
This article has not been copyedited and formatted. The final version may differ from this version.

Primary antibodies were diluted 1:200 (ARF6 antibody) or 1:800 (β-actin antibody) in PBS-T containing 5 % milk powder. Thereafter, membranes were again washed with PBS-T (4 times, each time for 5 min), followed by incubation with secondary biotinylated horse anti mouse IgG (BA-2000) (Vector Laboratories, Burlingame, CA, USA) (diluted 1:1,500 in PBS-T containing 5 % milk powder), washed again with PBS-T (4 times, each time for 5 min), incubated with avidin and biotinylated horseradish peroxidase (HRP) from the "Vectastain ABC kit" (Vector Laboratories, Burlingame, CA, USA) both diluted 1:200 in PBS, and washed again with PBS-T (4 times, each time for 5 min). Finally, blots were developed with enhanced chemiluminescence (ECL) using ECL Hyperfilm (GE Healthcare, Freiburg, Germany). Intensities of presumed ARF6 bands and bands for β-actin were quantified densitometrically using "Image J" (National Institutes of Health, Bethesda, Maryland, USA), and referred to β-actin in corresponding samples.

Contraction assay

Contractility of cells was measured using the Floating Matrix Model version of the CytoSelect™ 24-Well Cell Contraction Assay Kit (Cell Biolabs, San Diego, CA, USA). Cells were cultured in T75 flasks for 72 h, before being trypsinized and resuspended in fresh RPMI medium to a dilution 5x 10^6 cells/ml. Each well of the 24-well plates provided with the kit was filled with a matrix plug, containing 100 µl of the trypsinized cell suspension and 400 µl of collagen gel working solution provided with the kit, which was mixed before filling to the wells. Following incubation for 1 h (37 °C, 5 % CO_2) and collagen polymerization during this incubation, 1 ml RPMI medium (containing either no NAV2729 or DMSO, or NAV2729 as indicated or DMSO in corresponding amounts) were added, and incubation was continued (37 °C, 5 % CO_2). For monitoring of collagen contraction, pictures were taken 1 h and 3 h after adding of RPMI (corresponding to 2 h and 4 h after trypsinization). Diameters and areas

Molecular Pharmacology Fast Forward. Published on August 4, 2021 as DOI: 10.1124/molpharm.121.000304
This article has not been copyedited and formatted. The final version may differ from this version.

of the collagen plugs and wells on pictures were quantified using Image J, resulting in values for a) changes of the plug diameter (in mm; Δ of whole well diameter and of plug diameter at indicated time points) b) ratios between the collagen-covered area and the area of the whole well. Both quantification methods have been recommended by the manufacturer, and were applied here for quantification of the same experiments.

Phalloidin staining

For comparisons of proliferation rates between cell lines, 10,000 cells of each line were placed in each well of a 16-well chambered coverslip (Thermo Scientific, Waltham, MA, USA), and cultured in FCS-free medium. Cells were fixed with ROTI® Histofix 4 % solution (Roth, Karlsruhe, Germany) after 72 h of culture, and staining with 100 µM FITC-labelled phalloidin (Sigma-Aldrich, Munich, Germany) was performed in each well, according to the manufacturer's instruction. Labelled cells were analysed using a laser scanning microscope (Leica SP2, Wetzlar, Germany). Finally, all stainings were quantified using "Image J" (National Institutes of Health, Bethesda, Maryland, USA). To assess effects of NAV2729, again 10,000 cells were placed in each well of 16-well chambered coverslips, and incubated 24 h. Subsequently, NAV2729 or DMSO were added as indicated, followed by incubation for further 24 h without or with NAV2729 or DMSO. Finally, cells were fixed, stained and analyzed as described above.

Proliferation assay

Molecular Pharmacology Fast Forward. Published on August 4, 2021 as DOI: 10.1124/molpharm.121.000304
This article has not been copyedited and formatted. The final version may differ from this version.

Proliferation rate of cells was assessed using the 5-ethynyl-2'-deoxyuridine- (EdU-)based EdU-Click 555 proliferation assay kit (Baseclick, Tutzing, Germany), which was applied according to the manufacturer's instructions. In this assay, incorporation of EdU into DNA of proliferating cells is assessed by detection with fluorescing 5-carboxytetramethylrhodamine (5-TAMRA). For comparisons of proliferation rates between cell lines, 10,000 cells of each line were placed in each well of a 16-well chambered coverslip (Thermo Scientific, Waltham, MA, USA), and cultured in FCS-free medium. EdU was added after 48 h as a 10 mM stock solution. 24 h later, cells were fixed with ROTI® Histofix 4 % solution (Roth, Karlsruhe, Germany). Counterstaining of all nuclei was performed with DAPI. Finally, analysis was performed by fluorescence microscopy (excitation: 546 nm; emission: 479 nm) using a laser scanning microscope (Leica SP2, Wetzlar, Germany). Stainings were quantified using "Image J" (National Institutes of Health, Bethesda, Maryland, USA). To assess effects of NAV2729, again 10,000 cells were placed in each well of 16-well chambered coverslips, and cultured for 24 h in FCS-free medium, before NAV2729 in indicated concentrations or DMSO in required amounts were added. After incubation for further 24 h, the medium was replaced by 10 mM EdU solution in FCS-free smooth muscle cell medium containing NAV2729 or DMSO.

Assessment of Ki-67 content

As an indicator of proliferation, Ki-67 mRNA content of cells was semi-quantitatively assessed by RT-PCR. Compared to resting cells (G(0) phase)), Ki-67 is upregulated during all active phases of the cell cycle and of mitosis (Scholzen and Gerdes, 2000). Consequently, it is a suitable marker for proliferation, and has been commonly assessed to monitor proliferation in various cell types, including airway and vascular smooth muscle cells, or WPMY-1 cells (Dai et al., 2019; Halwani et al., 2013; Yu et al., 2019). Cells were seeded

Molecular Pharmacology Fast Forward. Published on August 4, 2021 as DOI: 10.1124/molpharm.121.000304
This article has not been copyedited and formatted. The final version may differ from this version.

in 6-well plates and grown to 70 % confluency. Subsequently, NAV2729 or DMSO were added as indicated, 24 h before RNA isolation. RNA isolation and RT-PCR were performed as decribed below.

RT-PCR

RNA from cells was isolated by using the RNeasy Mini kit (Qiagen, Hilden, Germany) according to the manufacturer's instructions. RNA concentrations were measured spectrophotometrically. Reverse transcription to cDNA was performed with 1 µg of isolated RNA using the reverse transcription kit (Promega, Madison, WI, USA). Ki-67 and glyceraldehyde 3-phosphate dehydrogenase (GAPDH) mRNA was detected using a Roche Light Cycler (Roche, Basel, Switzerland). Ready-to-use primers were purchased from Qiagen (Hilden, Germany), based on the RefSeq accession numbers NM_001145966 for Ki-67 and NM_002046 for GAPDH. PCR reactions were performed in a volume of 25 µl containing 5 µl LightCycler® FastStart DNA MasterPlus SYBR Green I (Roche, Basel, Switzerland), 1 µl template, 1 µl primer, and 18 µl water. Denaturation was performed for 10 min at 95 °C, and amplification with 45 cycles of 15 sec at 95 °C followed by 60 sec at 60 °C. The specificity of primers and amplification was demonstrated by subsequent analysis of melting points, which revealed single peaks for each target. Results were expressed using the ΔΔCt method, where number of cycles (Ct) at which the fluorescence signal exceeded a defined threshold for GAPDH was subtracted from Ct values for Ki-67 (Ct_{Ki-67}-Ct_{GAPDH} = ΔCt), and values were calculated as $2^{-\Delta Ct}$ and normalized to the mean values of corresponding controls.

Cell apoptosis analysis

Molecular Pharmacology Fast Forward. Published on August 4, 2021 as DOI: 10.1124/molpharm.121.000304
This article has not been copyedited and formatted. The final version may differ from this version.

A flow cytometry-based annexin V allophycocyanin (APC) and 7-aminoactinomycin D (7-AAD) apoptosis detection kit (BD Biosciences, Franklin Lakes, NJ, USA) was used to detect apoptotic (annexin V-positive, 7-AAD-negative) and dead (annexin V-positive, 7-AAD-positive) cells. Cell death in annexin V-positive/7-AAD-positive cells may result from apoptosis or necrosis, which can not distinguished by this assay. For comparisons between cell lines, around 100,000 cells were seeded in 6-well plates. After 48 h, cells were washed with PBS and resuspended in annexin V binding buffer (BD Biosciences), followed by addition of 5 µl APC annexin V and 5 µl 7-AAD reagent to each sample. After incubation in the dark for 15 min at room temperature, 400 µl binding buffer were added to each sample before analysis by flow cytometry. To assess effects of NAV2729, the procedure was the same, but NAV2729 or DMSO were added 24 h after seeding into 6-well plates (=24 h before washing with PBS).

Viability assay

Viability was assessed using the Cell Counting Kit-8 (CCK-8) (Sigma-Aldrich, Munich, Germany). For comparisons of proliferation rates between cell lines, cells were seeded in 96-well plates (5,000 cells/well) and cultured for 48 h, 72 h, or 96 h. Finally, 10 µl of [2-(2-methoxy-4-nitrophenyl)- 3-(4-nitrophenyl)-5-(2,4-disulfophenyl)-2H-tetrazolium monosodium salt (WST-8) from the kit were added, and absorbance in each well was measured at 450 nm after incubation for 2 h at 37 °C. To assess effects of NAV2729, again 5,000 cells/well were seeded in 96-well plates and cultured for 24 h. Subsequently, NAV2729 in indicated concentrations or DMSO in required amounts were added, and cells were cultured for further 24 h until assessment. IC_{50} values for NAV2729 were calculated by curve fitting using

Molecular Pharmacology Fast Forward. Published on August 4, 2021 as DOI: 10.1124/molpharm.121.000304
This article has not been copyedited and formatted. The final version may differ from this version.

GraphPad Prism 6 (Statcon, Witzenhausen, Germany) and analyzed as described below, based on experiments including a concentration range of 1.25 µM to 15 µM. For curve fitting, OD values were normalized to the DMSO control (set to 100 %), which was not included in curve but set as maximum y value, as variations of non-normalized, maximum OD values impeded plausible results from curve fitting. Automatic curve fitting was performed separately for each single experiment, to obtain single values for each single experiment. Sigmoidal concentration response curves were fitted by non-linear regression, without predefined constraints for bottom, top or IC_{50} values, by ordinary fit, without weighting, and without chosing automatic outlier elimination.

Drugs and nomenclature

NAV2729 (3-(4-Chlorophenyl)-5-(4-nitrophenyl)-2-(phenylmethyl)pyrazolo[1,5-a]pyrimidin-7(4H)-one) is a small molecule inhibitor with assumed selectivity for ARF6, and was obtained from Tocris (Bristol, UK). The batch used here (2A/246293) was analyzed for quality control by the provider, and showed a purity of 99 % in high-performance liquid chromatography (HPLC). ^{1}H nuclear magnetic resonance (NMR) spectroscopy and mass spectrometry were both consistent with the structure, and contents of carbon, hydrogen and nitrogen found in microanalyses were consistent with theoretical values (carbon theoretical/found 65.72/65.65, hydrogen 3.75/3.69, nitrogen 12.26/12.24). The structure of NAV2729 has been made available in PubChem (PubChem ID 2257249), and in the supplementary material of a recent article (Benabdi et al., 2017). NAV2729 inhibits ARF6 by direct binding to ARF6 and preventing its activation by guanosine exchange factors (GEFs), as well as its spontaneous activation occuring partially without nucleotide binding to ARF6 (Yamauchi et al., 2017; Yoo et al., 2016). Consequently, ARF6 inhibition does not depend on the identity of GEFs, which

Molecular Pharmacology Fast Forward. Published on August 4, 2021 as DOI: 10.1124/molpharm.121.000304
This article has not been copyedited and formatted. The final version may differ from this version.

may vary between cell types (Hongu and Kanaho, 2014; Yamauchi et al., 2017). Stock solutions (10 mM) were prepared in DMSO, and stored at -20 °C until use.

Data and statistical analyses

Our study aimed to examine effects of 1) ARF6 knockout in human prostate stromal cells, and 2) of NAV2729 treatment on contraction and growth-related functions in human prostate stromal cells with ARF6 knockout, in corresponding control cells with ARF6 expression, and in the parental cell line, i. e. WPMY-1 cells. Following creation and selection of knockout and control clones, contraction, actin organization, proliferation, apoptosis and cell death, and viability were compared between control cell lines and knockout clones, and effects of NAV2729 treatment on the same parameters were examined in all cell lines. After creation and selection of knockout and control clones as described above, each series of experiments was pre-planned to include five independent experiments, what was abided in all series (except of Western blot analyses, for reasons described below). Despite this preset study design, criteria for a strict hypothesis-driven character are not met, for following reasons. Firstly, knockout and control clones were selected for further experiments, after results from sequencing were obtained. Consequently, large parts of the study were adapted to these initial results, what is a clear feature excluding a hypothesis-testing character (Michel et al., 2020). Secondly, experiments were performed without blinding. Thirdly, definition of clear null hypotheses was not possible. Accordingly and in line with recent guidelines for reporting data, data analysis and statistical methods, our study should be considered as exploratory (Michel et al., 2020). No data were omitted, with the exception of Western blot analyses, for reasons explained below. Samples in Ki-67 analyses were determined in duplicate by RT-PCR, while all other quantifications and values are based on single samples and single determinations.

Molecular Pharmacology Fast Forward. Published on August 4, 2021 as DOI: 10.1124/molpharm.121.000304
This article has not been copyedited and formatted. The final version may differ from this version.

According to the exploratory character, reported p values are descriptive but not hypothesis-testing. In line with recent guidelines recommending sparing use of p values and to focus on effect sizes instead of p values (Michel et al., 2020), reporting of p values was limited to most relevant comparisons. Consequently, comparisons between cell lines did not include parental cells but were limited to knockout and control clones, and no comparisons were performed withing the three control clones or within the three knockout clones. Again in order to use p values sparingly and to maintain an appropriate degree of clearness in presentation, control clones were summarized to one group (i. e., a cluster containing all values from all three clones, 15 values in total) for statistical analyses, and values for each knockout clone were compared to this control group. Considering that low p values do not necessarily reflect large effect sizes (Michel et al., 2020), p values are here reported as symbols instead of exact or approximated values. Multiple comparisons between cell lines were performed by one-way ANOVA with Dunnett's tests, which allows comparison of a number of groups with a single control group. Comparisons in series including more than one concentration of NAV2729 and a control group (DMSO) in each single experiment were again performed by one-way ANOVA with a Dunnett's test. Comparisons in series including only one concentration of NAV2729 and a control group (DMSO) were performed by a two-tailed Student's t-test, which allows comparison between two groups. All tests were performed using GraphPrism 6 (Statcon, Witzenhausen, Germany). Comparisons in experiments with DMSO and NAV2729 are based on paired samples, as each independent experiment included application of DMSO and NAV2729 (including all concentrations as indicated) to the same cell line in the same experiment. P values <0.05 were considered significant.

All data are presented in scatter plots (instead of bar graphs or concentration responses), including all single values and means together with images of representative experiments (if

Molecular Pharmacology Fast Forward. Published on August 4, 2021 as DOI: 10.1124/molpharm.121.000304
This article has not been copyedited and formatted. The final version may differ from this version.

applicable) and as recently recommended by guidelines for displaying data in experimental biology (Michel et al., 2020). As the focus of data presentation was on effect sizes and variabilities, exemplarily or relevant effect sizes in the text are reported as mean difference (MD) or as means of clone clusters (i. e., all three control clones and of knockout clones) with 95 % confidence intervals (CI), which were calculated using SPSS® version 20 (IBM SPSS Statistics, IBM Corporation, Armonk, New York, USA) and are presented in square brackets.

Western blot analyses were preplanned with a minimum number of seven experiments, as a minimum of n=5 independent experiments was generally intended for each series, but we assumed in advance that 1) some samples may be to small to allow Western blot analysis (i. e. do not provide 2x 20 µg, required for ARF6 and β-actin blots, in at least one sample of a series), 2) detection may fail in some samples, 3) blots may be unsuitable for quantification, e. g. due to artefacts, or 4) outliers may occur. Consequently, seven independent experiments were performed for Western blot analyses. In fact, 2) occurred in one experiment, where ARF6 bands in a control cell line remained to weak to allow conclusive densitometric quantification, and 3) occurred in another experiment, where streaks covered parts of the band areas, resulting in unclean blots and impeding conclusive densitometric quantification. Thus, although ARF6 bands in these blots showed the same pattern as the other blots, these experiments could not be included at all, and presented Western blot analyses are based on five of seven experiments. All samples from one series were analyzed in the same blot.

Molecular Pharmacology Fast Forward. Published on August 4, 2021 as DOI: 10.1124/molpharm.121.000304
This article has not been copyedited and formatted. The final version may differ from this version.

Results

ARF6 knockout generation in WPMY-1 cells

From 104 sequenced single cell clones, six met the criteria for further experimentation, including three different ARF6-expressing control clones (in the following referred to as control A3, control C6 and control D7, or together as monoclonal ARF6 control clones), one clone showing ARF6 knockout in one of three alleles (referred to as single ARF6 knockout C4, or single ARF6 knockout clone), and two clones showing ARF6 knockout in two of three alleles (referred to as double knockout B4 or B9, or together as double knockout clones). Knockout of ARF6 in knockout clones was verified by Western blot analyses (fig. 1).

Effects of NAV2729 and ARF6 knockout on cell contraction

Cell contractions were assessed by matrix contraction assays. Compared to ARF6-expressing cell lines (WPMY-1, and three monoclonal ARF6 control clones), all three knockout clones showed reduced contractions, as reflected by reduced changes in diameters of collagen matrix plugs and by increased gel areas (the latter normalized to well areas, and expressed as ratios of gel area/matrix area) (fig. 2A). Thus, within 1 h after adding of RPMI to assay wells, matrix plugs contracted by 1.51 mm [1.18 to 1.84] across all three ARF6-expressing control clones, but around 0.58 mm [0.2 to 0.96] in all three ARF6 knockout clones. Accordingly, average ratios between gel areas and well areas ranged around 0.83 [0.77 to 0.88] across all three ARF6-expressing control clones 1 h after adding of RPMI, but around 0.94 [0.91 to 0.96] in all three ARF6 knockout clones. Within 3 h after adding of

Molecular Pharmacology Fast Forward. Published on August 4, 2021 as DOI: 10.1124/molpharm.121.000304
This article has not been copyedited and formatted. The final version may differ from this version.

RPMI, matrix plugs contracted by 3.68 mm [3.56 to 3.8] across all three ARF6-expressing control clones, but around 2.43 mm [1.54 to 3.33] in all three ARF6 knockout clones. Accordingly, average ratios between gel areas and well areas ranged around 0.67 [0.6 to 0.74] across all three control clones 3 after adding of RPMI, but around 0.77 [0.74 to 0.81] across all three knockout clones.

In the next series, effects of NAV2729 were assessed in all cell lines, by comparison of plug diameters and areas following addition of DMSO or NAV2729 (fig. 2B, C). In all four ARF6-expressing cell lines, the changes in plug diameter were lower, and gel area/well area ratios were larger in cells exposed to NAV2729 compared to cells exposed to DMSO, which was observed 1 h and 3 h after adding of RPMI with DMSO or NAV2729 (5 µM) and reflects inhibition of contraction by NAV2729 (fig. 2B, C). Across all three ARF6-expressing control clones, matrix plugs contracted on average by 1.9 mm [1.32 to 2.47] within 1 h after application of DMSO, but around 0.66 [0.21 to 1.11] within 1 h after application of NAV2729. In contrast, matrix plugs contracted on average by 1.16 mm [0.11 to 2.22] within 1 h after application of DMSO, and around 1.16 [0.52 to 1.8] within 1 h after application of NAV2729 across all three knockout clones. Within 3 h after application of DMSO or NAV2729, matrix plugs contracted on average by 4.18 mm [2.84 to 5.52] after DMSO, but around 1.97 [0.99 to 2.96] after NAV2729 across all three ARF6-expressing control clones. In contrast, changes in diameters were again similar after application of DMSO and NAV2729 across all three knockout clones, averaging to 2.43 mm [1.93 to 2.92] within 3 h after application of DMSO, and around 2.06 [1.15 to 2.97] within 3 h after application of NAV2729.

Similar patterns were observed, if ratios between plug areas and well areas were calculated and compared between DMSO and NAV2729 groups (fig. 2A, B). Thus, average ratios between gel areas and well areas ranged around 0.78 [0.58 to 0.99] 1 h after application of

Molecular Pharmacology Fast Forward. Published on August 4, 2021 as DOI: 10.1124/molpharm.121.000304
This article has not been copyedited and formatted. The final version may differ from this version.

DMSO, but around 0.91 [0.84 to 0.98] 1 h after application of NAV2729. 3 h after application of DMSO, average ratios between gel areas and well areas ranged around 0.6 [0.57 to 0.62], but around 0.78 [0.67 to 0.89] 3 h after application of NAV2729 across all three control clones. 6 h after application of DMSO, average ratios between gel areas and well areas ranged around 0.49 [0.44 to 0.55], but around 0.67 [0.48 to 0.86] 6 h after application of NAV2729 across all three control clones. In all three knockout clones, effects of NAV2729 were widely reduced or lacking (fig. 2B). Across all three ARF6 knockout clones, average ratios between gel areas and well areas ranged around 0.85 [0.66 to 1] 1 h after application of DMSO, and around 0.85 [0.68 to 1] 1 h after application of NAV2729. 3 h after application of DMSO, average ratios between gel areas and well areas ranged around 0.69 [0.56 to 0.82], and around 0.75 [0.6 to 0.9] 3 h after application of NAV2729 across all three knockout clones. 6 h after application of DMSO, average ratios between gel areas and well areas ranged around 0.56 [0.49 to 0.63], and around 0.63 [0.51 to 0.76] 6 h after application of NAV2729 across all three knockout clones.

Effects of NAV2729 and ARF6 knockout on actin organization

Polymerized actin was visualized by phalloidin staining. In WPMY-1 cells and monoclonal ARF6 control clones, actin was organized to long filaments and bundles, showing parallel arrangement and forming elongated protrusions, with filaments from different cells overlapping each other after 72 h of culture (fig. 3A). Phalloidin-stained actin covered more than 50 % of microscopic fields in these cells (fig. 3A). This actin organization observed in parental cells and control clones was widely lost in all three ARF6 knockout clones (fig. 3A). Remaining actin in knockout clones formed short and thicker filaments, or was arranged around the nucleus and just forming jag-like structures (fig. 3A). In addition to these qualitative changes, the extent of actin-stained areas was lower compared to parental cells

Molecular Pharmacology Fast Forward. Published on August 4, 2021 as DOI: 10.1124/molpharm.121.000304
This article has not been copyedited and formatted. The final version may differ from this version.

and control clones. Phalloidin-stained areas covered more than 50 % of microscopic fields in all ARF6-expressing cell lines (mean 55 % [49 to 61] for the three control clones), but less than 40 % of microscopic fiels in all three Arf6 knockout clones (36 % [29 to 43]) (fig. 3A).

In parental cells and ARF6 control clones, application of NAV2729 (2.5 µM, 5 µM) for 24 h caused concentration-dependent breakdowns of actin organization, and reduced the content of phalloidin-stained areas (fig. 3B). At qualitative level, the breakdown of actin organization caused by NAV2729 was characterized by concentration-dependent loss of the drawn-out filament structure of stained actin (fig. 3B). Compared to corresponding, DMSO-treated controls, remaining actin formed shorter and broader protrusions instead of clear filaments following exposure to 2.5 µM NAV2729, while no protrusions were formed and actin was largely centred around nuclei following exposure to 5 µM NAV2729 (fig. 3B). Quantitative changes changes resulting from NAV2729 were similar in all four cell lines, and included reductions of actin-covered areas around 40 % by 2.5 µM NAV2729, and 70 % by 5 µM NAV2729 (fig. 3B). Across all three ARF6-expressing control clones, average actin-covered areas ranged around 53 % [44 to 63] after application of DMSO, but around 33 % [11 to 56] after application of 2.5 µM NAV2729 and around 15 % [7 to 23] after application of 5 µM NAV2729 (fig. 3B).

In contrast to parental WPMY-1 cells and control clones, NAV2729 was without effect on the remaining content of phalloidin-stained actin in single knockout clones and in both double allele knockout clones. At qualitative level, a loss of actin organization to filaments became obvious in solvent-treated knockout clones. Other than in DMSO-treated ARF6 knockout clones, actin did not form long and thin filaments. Remaining protrusions were short, forming jagged structures and resulting a star-like shape of cells. Similarly, remaining filaments in both double allele knockout clones did not form protrusions any more, but rather jags or

Molecular Pharmacology Fast Forward. Published on August 4, 2021 as DOI: 10.1124/molpharm.121.000304
This article has not been copyedited and formatted. The final version may differ from this version.

edges, giving the cells a triangeled shape. At quantitative level, 2.5 µM NAV2729 remained without effect on phalloidin-stained areas, while 5 µM NAV2729 reduced the phalloidin-stained areas by approximately 17 %. Across all three knockout clones, average actin-covered areas ranged around 45 % [28 to 61] after application of DMSO, and around 44 % [26 to 61] after application of 2.5 µM NAV2729 and around 37 % [23 to 51] after application of 5 µM NAV2729 (fig. 3B).

Effects of NAV2729 and ARF6 knockout on proliferation

Proliferation was assessed by EdU assays and semiquantitative comparisons of Ki-67 mRNA expression. Both readouts pointed to a reduced proliferation in all three knockout clones, compared to parental cells and ARF6 control clones. Average proliferation rates (=percentages of cells showing proliferation) ranged higher than 67 % in all four control cell lines (mean 69 % [64 to 74] across all three control clones), but amounted to 52 % in the single knockout clone, and below 47 % in both double knockout clones (48 % [39 to 57] across all three knockout clones) after 72 h of culture (fig. 4A). Differences of similar extent were observed for Ki-67 mRNA contents after 48 h of culture (fig. 5A). Average $2^{-\Delta Ct}$ values ranged between 0.09 to 0.11 in all four control cell lines (0.096 [0.082 to 0.111] across all three control clones), but amounted to 0.07 in the single knockout clone and ranged around 0.06 in both double knockout clones (0.065 [0.042 to 0.089] across all three knockout clones) (fig. 5A).

In parental cells and ARF6 control clones, application of NAV2729 (2.5 µM, 5 µM) for 48 h caused concentration-dependent inhibition of proliferation, resulting in virtually complete termination of proliferation activity by 5 µM NAV2729 in EdU assays (fig. 4B). Across all three

Molecular Pharmacology Fast Forward. Published on August 4, 2021 as DOI: 10.1124/molpharm.121.000304
This article has not been copyedited and formatted. The final version may differ from this version.

ARF6-expressing control clones, average percentages of proliferating cells ranged around 55 % [39 to 71] after application of DMSO, but around 44 % [41 to 47] after application of 2.5 µM NAV2729 and around 1.4 % [-0.2 to 2.9] after application of 5 µM NAV2729 (fig. 4B). In ARF6 knockout clones, application of NAV2729 (2.5 µM, 5 µM) for 48 h was without any effect on proliferation rates, apart from a small decrease after application of 5 µM to clones B4 (fig. 4B). Across all three ARF6 knockout clones, average percentages of proliferating cells ranged around 47 % [42 to 53] after application of DMSO, and around 46 % [38 to 55] after application of 2.5 µM NAV2729 and around 41 % [20 to 63] after application of 5 µM NAV2729 (fig. 4B).

Effects of 5 µM NAV2729 on proliferation were confirmed by assessment of Ki-67 mRNA content (fig. 5B). 5 µM NAV2729 reduced the content of Ki-67 mRNA in all cell lines, which was clearer and stronger in ARF6-expressing control cell lines compared to knockout clones (fig. 5B). Thus, following application of 5 µM NAV2729, relative $2^{-\Delta Ct}$ values ranged around 0.34 fold of corresponding DMSO controls [0.25 to 0.43] across all three ARF6-expressing control clones, but around 0.73 fold of corresponding DMSO controls [0.68 to 0.77] across all three ARF6 knockout clones (fig. 5B).

Effects of NAV2729 and ARF6 knockout on apoptosis and cell death

Numbers of apoptotic and of dead cells were assessed by flowcytometry using labeling for 7-AAD and annexin V. Compared to parental cells and ARF6 control clones, the percentage of apoptotic cells (annexin V-positive, 7-AAD-negative) and the percentage of dead cells (annexin V-positive, 7-AAD-positive, resulting either from apoptosis, or necrosis) were increased in all three knockout clones after 48 h of culture. While the average percentage of

Molecular Pharmacology Fast Forward. Published on August 4, 2021 as DOI: 10.1124/molpharm.121.000304
This article has not been copyedited and formatted. The final version may differ from this version.

apoptotic cells did not exceed 5 % in control cell lines (mean 3.8 % [1.7 to 5.9] across all three control clones), it exceeded 18 % in all three knockout clones (20.4 % [11.4 to 29.4] across all three knockout clones) (fig. 6A). Similarly, the percentage of dead cells ranged below 6 % in all three control cell lines (4.5 % [2.7 to 6.3] across all three control clones), but above 15 % in all three knockout clones (17.4 % [13.3 to 21.6] across all three control clones) (fig. 6A).

Similar rates were observed in cells treated with DMSO, as controls for NAV2729 (fig. 6B). Application of NAV2729 (5 µM) for 24 h increased the percentages of apoptotic and dead cells in all four control cell lines with ARF6 expression, but not in ARF6 knockout clones (fig. 6B). Thus, across all three ARF6-expressing control clones, the average percentage of apoptotic cells ranged around 3 % [1.4 to 4.8] after treatment with DMSO, but around 15 % [13 to 17] after treatment with NAV2729 (fig. 6B). Across all three ARF6 knockout clones, the average percentage of apoptotic cells ranged around 22 % [-10 to 54] after treatment with DMSO, and around 19 % [-20 to 58] after treatment with NAV2729 (fig. 6B). Similarly and across all three ARF6-expressing control clones, the average percentage of dead cells ranged around 5 % [1.5 to 8.7] after treatment with DMSO, but around 31 % [17 to 46] after treatment with NAV2729 (fig. 6B). Across all three ARF6 knockout clones, the average percentage of dead cells ranged around 21 % [9 to 33] after treatment with DMSO, and around 25 % [16 to 35] after treatment with NAV2729 (fig. 6B).

Effects of NAV2729 and ARF6 knockout on viability

Viability of cells was assessed by CCK-8 assays, and increased with culture time (48-96 h), at least in ARF6-expressing control cell lines (fig. 7). The viability was lower in all three ARF6

Molecular Pharmacology Fast Forward. Published on August 4, 2021 as DOI: 10.1124/molpharm.121.000304
This article has not been copyedited and formatted. The final version may differ from this version.

knockout clones compared to parental cells and ARF6 control clones, what was best obvious after 72 h and 96 h of culture (fig. 7). Across all three ARF6-expressing control clones, average OD values ranged around 0.78 [0.76 to 0.80], but around 0.46 [0.21 to 0.70] across all three knockout clones after 72 h of culture. After 96 h of culture, average ratios between OD values ranged around 1.35 [1.32 to 1.39] across all three control clones, but around 0.51 [0.06 to 0.96] across all three knockout clones.

In cells with ARF6 expression, application of NAV2729 (24 h) caused concentration-dependent decreases in viability, with similar patterns in WPMY-1 cells and all three monoclonal ARF6 control clones. Thus, decreases in viability were observed using all concentrations (1 µM – 6.5 µM), starting with moderate or slight decreases at 1 µM, while 6.5 µM nearly completely reduced viability (fig. 8A). Accross all three ARF6-expressing control clones and compared to the corresponding DMSO-treated controls, 1 µM reduced the OD values by 26 % [7 to 44], 2.5 µM by 45 % [19 to 70], 5 µM by 82 % [71 to 93], and 6.5 µM by 91 % [86 to 97] (fig. 8A). Accross all three ARF6 knockout clones and compared to the corresponding DMSO-treated controls, 1 µM reduced the OD values by 1.8 % [-26 to 29], 2.5 µM by 11 % [-24 to 45], 5 µM by 50 % [-2 to 101], and 6.5 µM by 77 % [43 to 111] (fig. 8A).

Considering the concentration-dependent effects in these experiments, calculation of of IC_{50} values for NAV2729 appeared in principle possible, but was limited by the uncertainty whether maximum effects were attained in the applied concentration range. In order to calculate IC_{50} values for NAV2729, effects on viability were assessed using a broader concentration range from 1.25 µM to 15 µM (fig. 7C. In this range, NAV2729 completely inhibited viability in all cell lines (fig. 8B). Calculation of IC_{50} values by curve fitting pointed to increased IC_{50} values for NAV2729 in ARF6-expressing cell lines compared to knockout clones. Thus, IC_{50} values amounted to 3.2 µM [2.8 to 3.5] in paretal WPMY-1 cells, 3.3 µM [3

Molecular Pharmacology Fast Forward. Published on August 4, 2021 as DOI: 10.1124/molpharm.121.000304
This article has not been copyedited and formatted. The final version may differ from this version.

to 3.6] in control clone A3, 3.7 µM [2.6 to 4.8] in control clone C6 and 3.0 µM [2.4 to 3.6] in control clone D7, but to 8.2 µM [7.4 to 9] in knockout clone C4, 4.5 µM [4.1 to 4.9] in knockout clone B4 and 5 µM [4.2 to 5.7] in knockout clone B9 (fig. 8B).

Molecular Pharmacology Fast Forward. Published on August 4, 2021 as DOI: 10.1124/molpharm.121.000304
This article has not been copyedited and formatted. The final version may differ from this version.

Discussion

Our findings point to a role of ARF6 in promotion of contraction and proliferation, and in suppression of apoptosis in prostate stromal cells, and suggest a high specificity of the presumed ARF6 inhibitor NAV2729 within defined concentration ranges. To the best of our knowledge, this is the first evidence supporting a role of ARF6 in smooth muscle contraction using a knockout model. ARF6-mediated proliferation and suppression of apoptosis may both be involved in stromal growth and hyperplasia. In BPH, prostate smooth muscle contraction and stromal growth contribute to LUTS. Combination therapies are commonly applied to address contraction and growth at once in BPH. Here, both were targeted by NAV2729 in vitro. As other, established mediators of smooth muscle contraction are shared by different types of smooth muscle, investigation of similar ARF6 functions in other smooth muscle-rich organs merits further attention.

Compared to ARF6-expressing control clones, ARF knockout clones showed reduced contractions, impaired actin organization, decreased proliferation, increased apoptosis and cell death, and reduced overall survival. The possibly strongest of these changes were the increases in apoptosis and cell death. Previous evidence for ARF6-mediated suppression of apoptosis and cell death is limited, but available from prostate cancer cells, T cells, glioblastoma and osteosarcoma cells, and *Caenorhabditis elegans*, and included suppression of apoptosis and nonapoptotic cell death by ARF6 (Bhanot et al., 2010; Kutscher et al., 2018; Lei et al., 2020; Sumiyoshi et al., 2021). Cell death in annexin V-positive/7-AAD-positive cells detected in our flowcytometry analyses may result either from apoptosis or necrosis. Assuming that the difference between dead (annexin V-positive/7-AAD-positive) and apoptotic cells (annexin V-positive/7-AAD-negative) may mostly represent necrosis, our findings may suggest that cell death in knockout clones was predominantly or

Molecular Pharmacology Fast Forward. Published on August 4, 2021 as DOI: 10.1124/molpharm.121.000304
This article has not been copyedited and formatted. The final version may differ from this version.

nearly exclusively caused by apoptosis, and that the contribution of necrosis may have been small or even neglectable. In fact, the results from all three knockouts are very similar and may confirm each other to this regard. After application of NAV2729 to control clones, the number of dead cells exceeded the number of apoptotic cells (roughly 2-fold), so that necrosis may have been involved in NAV2729 effects in control clones. This divergence between ARF6 knockout clones and NAV2729-treated control clones can be hardly interpreted without speculations. In contrast to some other series, where different concentrations of NAV2729 were applied, NAV2729 was applied only at a single concentration (5 µM) in our flowcytometry experiments, what may limit comparisons between untreated knockout clones and NAV2729-treated control clones. Focussing on the definitive conclusions, we observed that a) ARF6 knockout strongly increased cell death and apoptosis, both parameters to similar degree, b) that NAV2729 increased both in control clones, but c) not at all in knockout clones.

In parallel to increased apoptosis, ARF6 knockout resulted in a reduced proliferation rate, and in reduced mRNA expression of the proliferation marker Ki-67. ARF6-mediated proliferation has been documented for several cell types, including cancer cells and vascular smooth muscle cells (Bourmoum et al., 2016; Charles et al., 2018; Li et al., 2017). Our current findings from ARF6 knockout clones confirm our previous findings that silencing of ARF6 expression by transfection with siRNA reduced proliferation of WPMY-1 cells (Yu et al., 2019). ARF6 may drive survival of prostate stromal cells by dual contributions of ARF6-mediated proliferation and ARF6-mediated suppression of apoptosis, finally resulting in the reduced viability of knockout clones observed in viability assays. Together, it appears possible, that ARF6 promotes stromal growth or prostate enlargement in BPH. In fact, BPH includes stromal hyperplasia, which may contribute to prostatic enlargement alone or together with epithelial hyperplasia (Strand et al., 2017).

Molecular Pharmacology Fast Forward. Published on August 4, 2021 as DOI: 10.1124/molpharm.121.000304
This article has not been copyedited and formatted. The final version may differ from this version.

ARF6 knockout clones showed reduced contractions in contractility assays, indicating a procontractile function of ARF6 in our cells. The parental cell line, i. e. WPMY-1 cells were derived from the prostate stroma, where smooth muscle cells are the predominant cell type. WPMY-1 cells show characteristics of prostate smooth muscle cells, including expression of α-smooth muscle actin, calponin and α_{1A}-adrenoceptors, while markers characteristic for epithelial, glandular cells are not detectable (Wang et al., 2016; Wang et al., 2015; Webber et al., 1999). Reduced contractions in knockout clones were paralleled by impaired actin organization. The latter may well account for reduced contractions in knockouts, as it is critical for contraction of any type of smooth muscle (Hennenberg et al., 2014; Puetz et al., 2009). Actin organization has been proposed as a major function of ARF6 (Donaldson, 2002; Humphreys et al., 2013; Klein et al., 2006; Luton, 2005; Schafer et al., 2000). In fact, other actin-dependent processes are susceptible to ARF6 inhibition or silencing as well, including migration of vascular smooth muscle cells (Charles et al., 2019; Charles et al., 2018; Charles et al., 2016).

A role of ARF6 in prostate smooth muscle contraction is in line with analog functions of other monomeric GTPases in smooth muscle contraction, which are emerging or already well-established (Li et al., 2020b). RhoA-mediated smooth muscle contraction is widely accepted and proven for probably any smooth muscle type (Somlyo and Somlyo, 2003). More recently, similar roles in smooth muscle contraction have been proposed for other monomeric GTPases (Li et al., 2020b). In particular for Rac GTPases, a role in smooth muscle contraction in different organs becomes increasingly obvious (Li et al., 2020b). Other non-RhoA GTPases with supposed roles in regulation of smooth muscle contraction include RasGTPases, Rap1b, Rab11A, Rab35, and Cdc42 (Li et al., 2020b). It may be speculated, that promotion of smooth muscle contraction by ARF6 is not limited to prostate smooth

Molecular Pharmacology Fast Forward. Published on August 4, 2021 as DOI: 10.1124/molpharm.121.000304
This article has not been copyedited and formatted. The final version may differ from this version.

muscle, but may occur in other smooth muscle-rich organs as well. Considering the high clinical relevance of smooth muscle contraction for pathophysiology and medical treatment of wide-spread diseases, investigation of ARF6 or NAV2729 in vascular, airway, and other smooth muscles appears reasonable.

In previous studies, NAV2729 showed IC_{50} values of 1 µM and 3.4 µM for ARF6 inhibition in fluorometric and orthogonal radiometric nucleotide exchange assays, but did not inhibit other ARF family members or other GTPases (Yoo et al., 2016). Calculation of IC_{50} values from our experiments addressing effects of NAV2729 on viability point to IC_{50} values between 3-3.7 µM in ARF6-expressing control cell lines, which were increased to 4.5-8.2 µM in knockout clones. Similarly, IC50 values around 2-3 µM may be estimated from our experiments based on phalloidin staining and EdU assays in ARF6-expressing cell lines, while effects by 5 µM NAV2729 were completely or nearly abolished in knockout cells in these experiments. In previous studies, a high degree of specificity for ARF6 has been proposed for NAV2729. Thus, NAV2729 was presumed to act with high specificity and selectivity of ARF6 even at concentrations of 50 µM, as neither RhoA, Rac1, H-Ras, Cdc42, or other ARF family members were inhibited in nucleotide exchange assays (Yoo et al., 2016). Application of 5 µM NAV2729 to WPMY-1 cells in our previous study inhibited ARF6, but not ARF1, Rac1 or RhoA (Yu et al., 2019). On the other hand, the specifity for ARF6 was challenged by a study reporting inhibition of ARF1 by 25 µM NAV2729 in nucleotide exchange assays, by inhibition of an ARF-GEF (Benabdi et al., 2017). However, effects of 5 µM NAV2729 in prostate tissues were not mimicked by the ARF1 inhibitor brefeldin A, so that ARF1 inhibition does not occur or is not relevant at concentrations up to 5 µM in prostate cells (Benabdi et al., 2017). In some series with knockout clones, we observed small effects using 5 µM to 15 µM NAV2729, what may refelect off-target effects at concentrations ≥5 µM, but may be explained by inhibition of remaining ARF6 as well.

Molecular Pharmacology Fast Forward. Published on August 4, 2021 as DOI: 10.1124/molpharm.121.000304
This article has not been copyedited and formatted. The final version may differ from this version.

As we observed that NAV2729 showed strong effects using concentrations up to 5 µM in ARF6-expressing cells, which were widely lacking in ARF6 knockout clones, we assume that NAV2729 acts mostly without off-target effects and ARF6-specific at concentrations up to 5 µM in our cells. In ARF6-expressing clones, 5 µM and lower concentrations showed large effects on contractility, actin organization, proliferation, apoptosis and cell death, and viability. In contrast, no or only small effects were observed using the same concentrations in knockout clones. Concentrations below 5 µM showed clear effects in some experiments with ARF6-expressing cells, which were completely blunted in knockout cells. Consequently, NAV2729 is obviously specific for ARF6, at least at concentrations up to 5 µM in our cells. Apparently, NAV2729 inhibits proliferation, survival and contraction, and increases apoptosis and cell death in prostate stromal by specific inhibition of ARF6, while contributions from off-target inhibition to these effects may be neglectable or lacking. Taking this specificty into account, it appears likely that the recently described inhibition of prostate smooth muscle contraction in human tissues by 5 µM NAV2729 was in fact caused by inhibition of ARF6 (Yu et al., 2019). Previous evidence suggesting inhibition of proliferation by NAV2729 in any cell type is surprisingly rare, if not limited to our previous findings obtained with WPMY-1 cells (Yu et al., 2019).

Overall, the effect of ARF6 knockout was remarkably similar between knockout at one allele compared to knockouts at two alleles. Generally, it is aimed to knockout all alleles in a cell, in order to obtain complete and clean knockout. Even though our clones were monoclonized by two consecutive single cell dilutions and monoclonality was assured, all clones still showed three alleles in the Miseq analysis. The results indicate that the cell line itself is not diploid, but triploid, in line with previous characterization of the parental cell line (Webber et al., 1999). Impurities or insufficient sequencing in the Miseq analysis can be excluded as two

Molecular Pharmacology Fast Forward. Published on August 4, 2021 as DOI: 10.1124/molpharm.121.000304
This article has not been copyedited and formatted. The final version may differ from this version.

independent rounds of sequencing showed the same output. In fact, we expected a stronger knockout phenotype in clones where two out of three alleles were knocked out compared to those where only one out of three alleles was knocked out. The lacking functional difference between one or two out of three knocked out alleles may indicate that already interrupting the Arf6 sequence in one allele is sufficient to lower the ARF6 protein expression drastically and that the remaining intact alleles are not sufficient to compensate the missing one. Another possibility could be off-target effects from the guideRNA. Even though there was no indel detected at the site of editing for the grey piechart alleles, successful ARF6 protein expression could be impaired by off-target effects from the guideRNA in regions close or in the Arf6 sequence, but outside the detection frame from the Miseq analysis.

Together, our findings suggest a dual role of ARF6 for smooth muscle contraction and stromal growth in the prostate. Identifying the involved molecular mechanims merits further attention by future studies. Smooth muscle contraction and stromal can both contribute to urethral obstruction in BPH, resulting in impaired bladder empyting and voiding, and finally in LUTS suggestive of BPH (Hennenberg et al., 2014). Accordingly, both factors are important targets for medical therapy (Hennenberg et al., 2014; Oelke et al., 2013). Combination therapies are applied to address both processes at once (Fullhase et al., 2013; Oelke et al., 2013). For decades, smooth muscle contraction and growth in BPH were mostly considered separately. Obviously, both are not independent players in driving LUTS, as previously assumed, but rather linked with each other by ARF6. Similar connections between contraction and proliferation are well evidenced in other context, with RhoA/Rho kinase mediating both process in vascular smooth muscle probably as one of the best examples (Shimokawa et al., 2016).

Molecular Pharmacology Fast Forward. Published on August 4, 2021 as DOI: 10.1124/molpharm.121.000304
This article has not been copyedited and formatted. The final version may differ from this version.

For treatment of voiding symptoms, α_1-adrenoceptor antagonists and the phosphodiesterase-5 inhibitor tadalafil are available (Oelke et al., 2013). Both may improve maximum urinary flow rate and symptom scores by relaxation of prostate smooth muscle (Oelke et al., 2013). For prevention of progression and complications, 5α-reductase inhibitors are applied, which may reduce prostate size by inhibition of testosteron-dependent growth (Oelke et al., 2013). However, improvements of symptoms and urinary flow rate are limited to 40-50 %, while even placebos may show improvements around 30 % and the percentage of non-responders amounts up to 30-35 % (Chapple et al., 2011; Eredics et al., 2017; Kortmann et al., 2003; Madersbacher et al., 2007). Combination therapies are, in turn, characterized by low tolerability, and show no additive benefits regarding the improvements of symptoms and urinary flow (Fullhase et al., 2013). Consequently, discontinuation due to unbalanced side effects and disappointing efficacy is common, amounting up to 65 % within one year even for monotherapy with α_1-adrenoceptor antagonists, and accounting for progression, complications, hospitalization, and surgery for BPH (Cindolo et al., 2015a; Cindolo et al., 2015b). Thus, novel medications may be appreciated, and identification of molecular mechanisms with dual functions in contraction and growth in BPH may offer novel perspectives to develop single compounds targeting both at once. At least in vitro, both processes were inhibited by NAV2729 in our study, demonstrating that such compounds are in principle available.

Conclusions

ARF6 promotes smooth muscle contraction and proliferation in the human prostate stroma. Both can be inhibited by NAV2729, which acts without off-target effect up to 5 µM in prostate stromal role. ARF6 merits further investigation in the context of smooth muscle contraction in other smooth muscle-rich organs.

Molecular Pharmacology Fast Forward. Published on August 4, 2021 as DOI: 10.1124/molpharm.121.000304
This article has not been copyedited and formatted. The final version may differ from this version.

Molecular Pharmacology Fast Forward. Published on August 4, 2021 as DOI: 10.1124/molpharm.121.000304
This article has not been copyedited and formatted. The final version may differ from this version.

Acknowledgments

We thank Prof. Dr. Veit Hornung and Stefan Bauernfried (Gene Center and Department of Biochemistry, LMU Munich, Munich, Germany) for providing us plasmids, and their support with separation of transfected cells and sequencing. We thank Prof. Dr. Elfriede Noessner and her coworkers (Institute of Molecular Immunology, Helmholtz Center, Munich) for their support with immunofluorescence microscopy.

Authorship Contributions

Participated in research design: Wang, Keppler, Stief, Hennenberg. Conducted experiments: Wang, Schneider, Li, Rutz, Ciotkowska, Hennenberg. Performed data analysis: Wang, Schneider, Li, Rutz, Ciotkowska, Hennenberg. Wrote or contritubed to the writing of the manuscript: Wang, Schneider, Keppler, Stief, Hennenberg.

Molecular Pharmacology Fast Forward. Published on August 4, 2021 as DOI: 10.1124/molpharm.121.000304
This article has not been copyedited and formatted. The final version may differ from this version.

References

Benabdi S, Peurois F, Nawrotek A, Chikireddy J, Caneque T, Yamori T, Shiina I, Ohashi Y, Dan S, Rodriguez R, Cherfils J and Zeghouf M (2017) Family-wide Analysis of the Inhibition of Arf Guanine Nucleotide Exchange Factors with Small Molecules: Evidence of Unique Inhibitory Profiles. *Biochemistry* **56**(38): 5125-5133.

Bhanot H, Young AM, Overmeyer JH and Maltese WA (2010) Induction of nonapoptotic cell death by activated Ras requires inverse regulation of Rac1 and Arf6. *Mol Cancer Res* **8**(10): 1358-1374.

Bourmoum M, Charles R and Claing A (2016) The GTPase ARF6 Controls ROS Production to Mediate Angiotensin II-Induced Vascular Smooth Muscle Cell Proliferation. *PLoS One* **11**(1): e0148097.

Chapple CR, Montorsi F, Tammela TL, Wirth M, Koldewijn E, Fernandez Fernandez E and European Silodosin Study G (2011) Silodosin therapy for lower urinary tract symptoms in men with suspected benign prostatic hyperplasia: results of an international, randomized, double-blind, placebo- and active-controlled clinical trial performed in Europe. *Eur Urol* **59**(3): 342-352.

Charles R, Bourmoum M, Campbell S and Claing A (2019) Methods to Investigate the beta-Arrestin-Mediated Control of ARF6 Activation to Regulate Trafficking and Actin Cytoskeleton Remodeling. *Methods Mol Biol* **1957**: 159-168.

Charles R, Bourmoum M and Claing A (2018) ARF GTPases control phenotypic switching of vascular smooth muscle cells through the regulation of actin function and actin dependent gene expression. *Cell Signal* **46**: 64-75.

Charles R, Namkung Y, Cotton M, Laporte SA and Claing A (2016) beta-Arrestin-mediated Angiotensin II Signaling Controls the Activation of ARF6 Protein and Endocytosis in Migration of Vascular Smooth Muscle Cells. *J Biol Chem* **291**(8): 3967-3981.

Choi WH, Kim J, Lee YR, Lee CK, Kim YS, Kim J, Choi YJ, Woo NS, Cho S and Kim B (2005) Cdc42 contributes to phorbol ester-induced Ca2+-independent contraction of pulmonary artery smooth muscle. *J Vet Med Sci* **67**(8): 787-793.

Cindolo L, Pirozzi L, Fanizza C, Romero M, Tubaro A, Autorino R, De Nunzio C and Schips L (2015a) Drug adherence and clinical outcomes for patients under pharmacological therapy for lower urinary tract symptoms related to benign prostatic hyperplasia: population-based cohort study. *Eur Urol* **68**(3): 418-425.

Cindolo L, Pirozzi L, Sountoulides P, Fanizza C, Romero M, Castellan P, Antonelli A, Simeone C, Tubaro A, de Nunzio C and Schips L (2015b) Patient's adherence on pharmacological therapy for benign prostatic hyperplasia (BPH)-associated lower urinary tract symptoms (LUTS) is different: is combination therapy better than monotherapy? *BMC Urol* **15**: 96.

D'Souza-Schorey C and Chavrier P (2006) ARF proteins: roles in membrane traffic and beyond. *Nat Rev Mol Cell Biol* **7**(5): 347-358.

Dai F, Qi Y, Guan W, Meng G, Liu Z, Zhang T and Yao W (2019) RhoGDI stability is regulated by SUMOylation and ubiquitination via the AT1 receptor and participates in Ang II-induced smooth muscle proliferation and vascular remodeling. *Atherosclerosis* **288**: 124-136.

Donaldson JG (2002) Arf6 and its role in cytoskeletal modulation. *Methods Mol Biol* **189**: 191-198.

Eredics K, Madersbacher S and Schauer I (2017) A Relevant Midterm (12 Months) Placebo Effect on Lower Urinary Tract Symptoms and Maximum Flow Rate in Male Lower Urinary Tract Symptom and Benign Prostatic Hyperplasia-A Meta-analysis. *Urology* **106**: 160-166.

Fullhase C, Chapple C, Cornu JN, De Nunzio C, Gratzke C, Kaplan SA, Marberger M, Montorsi F, Novara G, Oelke M, Porst H, Roehrborn C, Stief C and McVary KT (2013)

Systematic review of combination drug therapy for non-neurogenic male lower urinary tract symptoms. *Eur Urol* **64**(2): 228-243.

Gauthier-Campbell C, Bredt DS, Murphy TH and El-Husseini Ael D (2004) Regulation of dendritic branching and filopodia formation in hippocampal neurons by specific acylated protein motifs. *Mol Biol Cell* **15**(5): 2205-2217.

Halwani R, Vazquez-Tello A, Sumi Y, Pureza MA, Bahammam A, Al-Jahdali H, Soussi-Gounni A, Mahboub B, Al-Muhsen S and Hamid Q (2013) Eosinophils induce airway smooth muscle cell proliferation. *J Clin Immunol* **33**(3): 595-604.

Hennenberg M, Stief CG and Gratzke C (2014) Prostatic alpha1-adrenoceptors: new concepts of function, regulation, and intracellular signaling. *Neurourol Urodyn* **33**(7): 1074-1085.

Hiroi T, Someya A, Thompson W, Moss J and Vaughan M (2006) GEP100/BRAG2: activator of ADP-ribosylation factor 6 for regulation of cell adhesion and actin cytoskeleton via E-cadherin and alpha-catenin. *Proc Natl Acad Sci U S A* **103**(28): 10672-10677.

Hongu T and Kanaho Y (2014) Activation machinery of the small GTPase Arf6. *Adv Biol Regul* **54**: 59-66.

Hongu T, Yamauchi Y, Funakoshi Y, Katagiri N, Ohbayashi N and Kanaho Y (2016) Pathological functions of the small GTPase Arf6 in cancer progression: Tumor angiogenesis and metastasis. *Small GTPases* **7**(2): 47-53.

Humphreys D, Davidson AC, Hume PJ, Makin LE and Koronakis V (2013) Arf6 coordinates actin assembly through the WAVE complex, a mechanism usurped by Salmonella to invade host cells. *Proc Natl Acad Sci U S A* **110**(42): 16880-16885.

Jones MC, Zha J and Humphries MJ (2019) Connections between the cell cycle, cell adhesion and the cytoskeleton. *Philos Trans R Soc Lond B Biol Sci* **374**(1779): 20180227.

Klein S, Franco M, Chardin P and Luton F (2006) Role of the Arf6 GDP/GTP cycle and Arf6 GTPase-activating proteins in actin remodeling and intracellular transport. *J Biol Chem* **281**(18): 12352-12361.

Kortmann BB, Floratos DL, Kiemeney LA, Wijkstra H and de la Rosette JJ (2003) Urodynamic effects of alpha-adrenoceptor blockers: a review of clinical trials. *Urology* **62**(1): 1-9.

Kutscher LM, Keil W and Shaham S (2018) RAB-35 and ARF-6 GTPases Mediate Engulfment and Clearance Following Linker Cell-Type Death. *Dev Cell* **47**(2): 222-238 e226.

Lei H, Ma F, Jia R and Tan B (2020) Effects of Arf6 downregulation on biological characteristics of human prostate cancer cells. *Int Braz J Urol* **46**(6): 950-961.

Li B, Wang R, Wang Y, Stief CG and Hennenberg M (2020a) Regulation of smooth muscle contraction by monomeric non-RhoA GTPases. *Br J Pharmacol*.

Li B, Wang R, Wang Y, Stief CG and Hennenberg M (2020b) Regulation of smooth muscle contraction by monomeric non-RhoA GTPases. *Br J Pharmacol* **177**(17): 3865-3877.

Li R, Peng C, Zhang X, Wu Y, Pan S and Xiao Y (2017) Roles of Arf6 in cancer cell invasion, metastasis and proliferation. *Life sciences* **182**: 80-84.

Luton F (2005) The role of EFA6, exchange factor for Arf6, for tight junction assembly, functions, and interaction with the actin cytoskeleton. *Methods Enzymol* **404**: 332-345.

Madersbacher S, Marszalek M, Lackner J, Berger P and Schatzl G (2007) The long-term outcome of medical therapy for BPH. *Eur Urol* **51**(6): 1522-1533.

Michel MC, Murphy TJ and Motulsky HJ (2020) New Author Guidelines for Displaying Data and Reporting Data Analysis and Statistical Methods in Experimental Biology. *Mol Pharmacol* **97**(1): 49-60.

Miura Y, Hongu T, Yamauchi Y, Funakoshi Y, Katagiri N, Ohbayashi N and Kanaho Y (2016) ACAP3 regulates neurite outgrowth through its GAP activity specific to Arf6 in mouse hippocampal neurons. *Biochem J* **473**(17): 2591-2602.

Oelke M, Bachmann A, Descazeaud A, Emberton M, Gravas S, Michel MC, N'Dow J, Nordling J, de la Rosette JJ and European Association of U (2013) EAU guidelines on the treatment and follow-up of non-neurogenic male lower urinary tract symptoms including benign prostatic obstruction. *Eur Urol* **64**(1): 118-140.

Puetz S, Lubomirov LT and Pfitzer G (2009) Regulation of smooth muscle contraction by small GTPases. *Physiology (Bethesda)* **24**: 342-356.

Schafer DA, D'Souza-Schorey C and Cooper JA (2000) Actin assembly at membranes controlled by ARF6. *Traffic* **1**(11): 892-903.

Schmid-Burgk JL, Schmidt T, Gaidt MM, Pelka K, Latz E, Ebert TS and Hornung V (2014) OutKnocker: a web tool for rapid and simple genotyping of designer nuclease edited cell lines. *Genome Res* **24**(10): 1719-1723.

Scholzen T and Gerdes J (2000) The Ki-67 protein: from the known and the unknown. *J Cell Physiol* **182**(3): 311-322.

Schweitzer JK and D'Souza-Schorey C (2005) A requirement for ARF6 during the completion of cytokinesis. *Exp Cell Res* **311**(1): 74-83.

Shimokawa H, Sunamura S and Satoh K (2016) RhoA/Rho-Kinase in the Cardiovascular System. *Circ Res* **118**(2): 352-366.

Somlyo AP and Somlyo AV (2003) Ca2+ sensitivity of smooth muscle and nonmuscle myosin II: modulated by G proteins, kinases, and myosin phosphatase. *Physiol Rev* **83**(4): 1325-1358.

Strand DW, Costa DN, Francis F, Ricke WA and Roehrborn CG (2017) Targeting phenotypic heterogeneity in benign prostatic hyperplasia. *Differentiation* **96**: 49-61.

Sumiyoshi M, Kotani Y, Ikuta Y, Suzue K, Ozawa M, Katakai T, Yamada T, Abe T, Bando K, Koyasu S, Kanaho Y, Watanabe T and Matsuda S (2021) Arf1 and Arf6

Synergistically Maintain Survival of T Cells during Activation. *J Immunol* **206**(2): 366-375.

Torii T, Miyamoto Y, Sanbe A, Nishimura K, Yamauchi J and Tanoue A (2010) Cytohesin-2/ARNO, through its interaction with focal adhesion adaptor protein paxillin, regulates preadipocyte migration via the downstream activation of Arf6. *J Biol Chem* **285**(31): 24270-24281.

Urban AE, Quick EO, Miller KP, Krcmery J and Simon HG (2016) Pdlim7 Regulates Arf6-Dependent Actin Dynamics and Is Required for Platelet-Mediated Thrombosis in Mice. *PLoS One* **11**(10): e0164042.

Wang Y, Gratzke C, Tamalunas A, Wiemer N, Ciotkowska A, Rutz B, Waidelich R, Strittmatter F, Liu C, Stief CG and Hennenberg M (2016) P21-Activated Kinase Inhibitors FRAX486 and IPA3: Inhibition of Prostate Stromal Cell Growth and Effects on Smooth Muscle Contraction in the Human Prostate. *PLoS One* **11**(4): e0153312.

Wang Y, Kunit T, Ciotkowska A, Rutz B, Schreiber A, Strittmatter F, Waidelich R, Liu C, Stief CG, Gratzke C and Hennenberg M (2015) Inhibition of prostate smooth muscle contraction and prostate stromal cell growth by the inhibitors of Rac, NSC23766 and EHT1864. *Br J Pharmacol* **172**(11): 2905-2917.

Webber MM, Trakul N, Thraves PS, Bello-DeOcampo D, Chu WW, Storto PD, Huard TK, Rhim JS and Williams DE (1999) A human prostatic stromal myofibroblast cell line WPMY-1: a model for stromal-epithelial interactions in prostatic neoplasia. *Carcinogenesis* **20**(7): 1185-1192.

Yamauchi Y, Miura Y and Kanaho Y (2017) Machineries regulating the activity of the small GTPase Arf6 in cancer cells are potential targets for developing innovative anti-cancer drugs. *Adv Biol Regul* **63**: 115-121.

Yoo JH, Shi DS, Grossmann AH, Sorensen LK, Tong Z, Mleynek TM, Rogers A, Zhu W, Richards JR, Winter JM, Zhu J, Dunn C, Bajji A, Shenderovich M, Mueller AL, Woodman SE, Harbour JW, Thomas KR, Odelberg SJ, Ostanin K and Li DY (2016)

ARF6 Is an Actionable Node that Orchestrates Oncogenic GNAQ Signaling in Uveal Melanoma. *Cancer Cell* **29**(6): 889-904.

Yu Q, Gratzke C, Wang R, Li B, Kuppermann P, Herlemann A, Tamalunas A, Wang Y, Rutz B, Ciotkowska A, Wang X, Strittmatter F, Waidelich R, Stief CG and Hennenberg M (2019) A NAV2729-sensitive mechanism promotes adrenergic smooth muscle contraction and growth of stromal cells in the human prostate. *J Biol Chem* **294**(32): 12231-12249.

Molecular Pharmacology Fast Forward. Published on August 4, 2021 as DOI: 10.1124/molpharm.121.000304
This article has not been copyedited and formatted. The final version may differ from this version.

Footnotes

This work was supported by the Deutsche Forschungsgemeinschaft [Grant HE 5825/8-1]; and the Chinese Scholarship Council (CSC) [Grants 201608210185 (RW), 201706370083 (BL)].

Molecular Pharmacology Fast Forward. Published on August 4, 2021 as DOI: 10.1124/molpharm.121.000304
This article has not been copyedited and formatted. The final version may differ from this version.

Legends to Figures

Figure 1: ARF6 knockout in WPMY-1 cells. Western blot analyses of parental cells (WPMY-1), ARF6-expressing monoclonal control clones (controls A3, C6, D7) and monoclonal ARF6 knockout clones (single allele knockout clone C4, and double allele knockout clones B4 and B9) were performed using an antibody raised against ARF6 and β-actin. In **(A)**, representative Western blots together with positions of a molecular weight marker, indicated expected sizes of detected proteins and piecharts are shown. Piecharts represent the MiSeq analysis of clones on the DNA level as well as the verification of triploidy in this particular cell line. Red and orange colors represent two different out of frame mutations at the site of editing. Grey piecharts mean that no indel (no change) was detected at the particular site of editing. The size of piecharts represents the number of reads in the sequencing and indicates that all clones showed sufficient sequencing reads. In **(B)**, all single values (ratios of band intensities as indicated) of all samples obtained from quantification of five independent experiments are shown. Values of each knockout clone were compared to a cluster containing all values of all control clones by one-way ANOVA with Dunnett's tests (** $p < 0.01$, *** $p<0.001$ vs. a control group composed of all values of A3, C6 and D7). Parental WPMY-1 cells were not included to statistical analyses.

Figure 2: Contraction of WPMY1 cells, ARF6 control clones and ARF6 knockout clones. Contractions were compared between cell lines **(A)**, and between cells exposed to DMSO or NAV2729 (5 µM) for 1 h **(B)** or 3 h **(C)**. Cells were seeded in matrix plugs, without or with DMSO or NAV2729, and areas of plugs and whole wells were assessed after indicated periods, following 1 h or 3 h after addition of RPMI with or without DMSO or NAV2729 to plugs. Separate series of experiments were performed to compare contraction between cell lines **(A)**, and to assess effects of NAV2729 in all cell lines in **(B)** and **(C)**. Results are

Molecular Pharmacology Fast Forward. Published on August 4, 2021 as DOI: 10.1124/molpharm.121.000304
This article has not been copyedited and formatted. The final version may differ from this version.

expressed as changes in plug diameter during indicated periods, and as ratios between plug area and whole well area. Contraction of cells reduces the diameters of matrix plugs, so that lower gel/well area ratios reflect higher contraction and higher gel/well area ratios reflect lower contraction. Consequently, gel/well area ratios are shown using y axes with reverse direction, to visualize higher and lower contractions. Shown are all single values together with means from five independent experiments for each setting. In **(A)**, values of each knockout clone were compared to a cluster containing all 15 values of all three control clones together by one-way ANOVA with Dunnett's tests (* $p<0.05$, ** $p< 0.01$, *** $p<0.001$ vs. a control group composed of all values of A3, C6 and D7). Parental WPMY-1 cells were not included to statistical analyses. In **(B)** and **(C)**, values from both groups were compared by two-tailed Student's t-test in each diagram (* $p<0.05$, ** $p< 0.01$, *** $p<0.001$ vs. DMSO).

Figure 3: Actin organization in WPMY1 cells, ARF6 control clones and ARF6 knockout clones. Phalloidin staining was performed, after cells were cultured for 72 h without **(A)**, or for 24 h with **(B)** DMSO or NAV2729 in indicated concentrations. Subsequently, actin polymers were stained by phalloidin, resulting in red staining of polyermized actin. Nuclei were counterstained with DAPI (blue). Separate series of experiments were performed to compare actin organization between cell lines in **(A)**, and to assess effects of NAV2729 in all cell lines in **(B)**. Shown are all single values together with means from quantification of phalloidin-stained actin in five independent experiments for each setting together with representative images for each setting. In **(A)**, values of each knockout clone were compared to a cluster containing all 15 values of all three control clones together by one-way ANOVA with Dunnett's tests (*** $p<0.001$ vs. a control group composed of all values of A3, C6 and D7). Parental WPMY-1 cells were not included to statistical analyses. In **(B)**, values of each NAV2729 group were compared by one-way ANOVA with Dunnett's tests to values of the corresponding DMSO group (* $p<0.05$, ** $p< 0.01$, *** $p<0.001$ vs. DMSO).

Molecular Pharmacology Fast Forward. Published on August 4, 2021 as DOI: 10.1124/molpharm.121.000304
This article has not been copyedited and formatted. The final version may differ from this version.

Figure 4: Proliferation in WPMY1 cells, ARF6 control clones and ARF6 knockout clones. Proliferation was assessed by EdU assays (red, proliferating cells; blue, non-proliferating cells), after cells were cultured for 72 h without **(A)**, or for 48 h with **(B)** DMSO or NAV2729 in indicated concentrations. Separate series of experiments were performed to compare proliferation between cell lines in **(A)**, and to assess effects of NAV2729 in all cell lines in **(B)**. Shown are all single values together with means from quantification of proliferating cells in five independent experiments together with representative images for each setting. In **(A)**, values of each knockout clone were compared to a cluster containing all 15 values of all three control clones together by one-way ANOVA with Dunnett's tests (*** $p<0.001$ vs. a control group composed of all values of A3, C6 and D7). Parental WPMY-1 cells were not included to statistical analyses. In **(B)**, values of each NAV2729 group were compared by one-way ANOVA with Dunnett's tests to values of the corresponding DMSO group (* $p<0.05$, ** $p< 0.01$, *** $p<0.001$ vs. DMSO).

Figure 5: Ki-67 mRNA content in WPMY1 cells, ARF6 control clones and ARF6 knockout clones. Ki-67 mRNA content was assessed by RT-PCR, after cells were cultured for 24 h with DMSO in required amounts, or NAV2729 in indicated concentrations. Data in **(A)** and **(B)** are derived from the same experiments, and include $2^{-\Delta Ct}$ values for comparison of Ki-67 content between the different cell lines in **(A)**, and $2^{-\Delta Ct}$ values normalized to the mean of the corresponding DMSO group to assess the effects of NAV2729 in each cell line in **(B)**. Shown are all single values together with means from five independent experiments. In **(A)**, values of each knockout clone were compared to a cluster containing all 15 values of all three control clones together by one-way ANOVA with Dunnett's tests (** $p< 0.01$, *** $p<0.001$ vs. a control group composed of all values of A3, C6 and D7). Parental WPMY-1 cells were not

Molecular Pharmacology Fast Forward. Published on August 4, 2021 as DOI: 10.1124/molpharm.121.000304
This article has not been copyedited and formatted. The final version may differ from this version.

included to statistical analyses. In **(B)**, values from both groups were compared by two-tailed Student's t-test in each diagram (* p<0.05, ** p< 0.01, *** p<0.001 vs. DMSO).

Figure 6: Apoptosis and cell death in WPMY1 cells, ARF6 control clones and ARF6 knockout clones. Flow cytometry was performed, after cells were cultured for 48 h without **(A)**, or for 24 h with **(B)** DMSO or NAV2729 in indicated concentrations. Subsequently, numbers of cells being in apoptosis (annexin V-positive, 7-AAD-negative), and of dead cells (resulting from apoptosis and/or necrosis; annexin V-positive, 7-AAD-positive) were assessed by flow cytometry. Separate series of experiments were performed to compare apoptosis and cell death between cell lines in **(A)**, and to assess effects of NAV2729 in all cell lines in **(B)**. Shown are all single values together with means from quantification of five independent experiments and representative experiments for each setting. In **(A)**, values of each knockout clone were compared to a cluster containing all 15 values of all three control clones together by one-way ANOVA with Dunnett's tests (*** p<0.001 vs. a control group composed of all values of A3, C6 and D7). Parental WPMY-1 cells were not included to statistical analyses. In **(B)**, values from both groups were compared by two-tailed Student's t-test in each diagram (* p<0.05, ** p< 0.01, *** p<0.001 vs. DMSO).

Figure 7: Viability of WPMY1 cells, control clones and ARF6 knockout clones, and IC_{50} values for NAV2729. Cell were cultured for indicated periods without **(A)**, or for 24 h with **(B,C)** DMSO or NAV2729 in indicated concentrations, before viability was assesed by CCK-8 assay. Based on experiments shown in **(C)**, IC_{50} values for NAV2729 were calculated for each cell line **(C)**. Separate series of experiments were performed to compare viability between cell lines in **(A)**, and to assess effects of NAV2729 in all cell lines in **(B,C)**. Shown are all single values together with means from quantification of five independent experiments for each setting. In **(A)** and for comparison of IC_{50} values between clones, values of each

Molecular Pharmacology Fast Forward. Published on August 4, 2021 as DOI: 10.1124/molpharm.121.000304
This article has not been copyedited and formatted. The final version may differ from this version.

knockout clone were compared to a cluster containing all 15 values of all three control clones together by one-way ANOVA with Dunnett's tests (** $p< 0.01$, *** $p<0.001$ vs. a control group composed of all values of A3, C6 and D7). Parental WPMY-1 cells were not included to statistical analyses. In **(B)** and **(C)** (except comparison of IC_{50} values), values of each NAV2729 group were compared by one-way ANOVA with Dunnett's tests to values of the corresponding DMSO group (* $p<0.05$, ** $p< 0.01$, *** $p<0.001$ vs. DMSO).

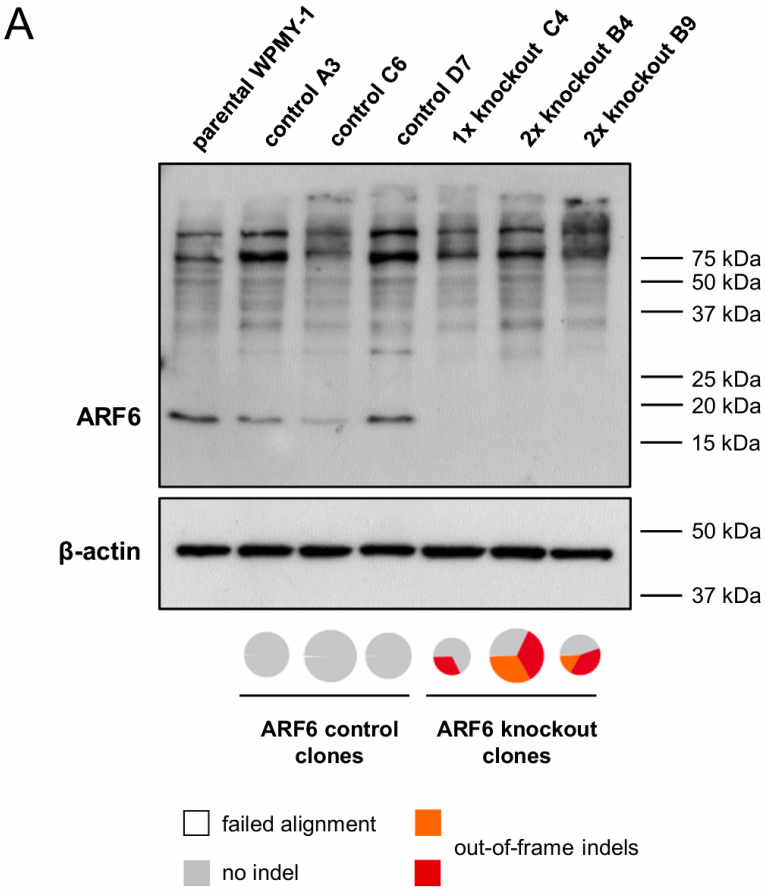

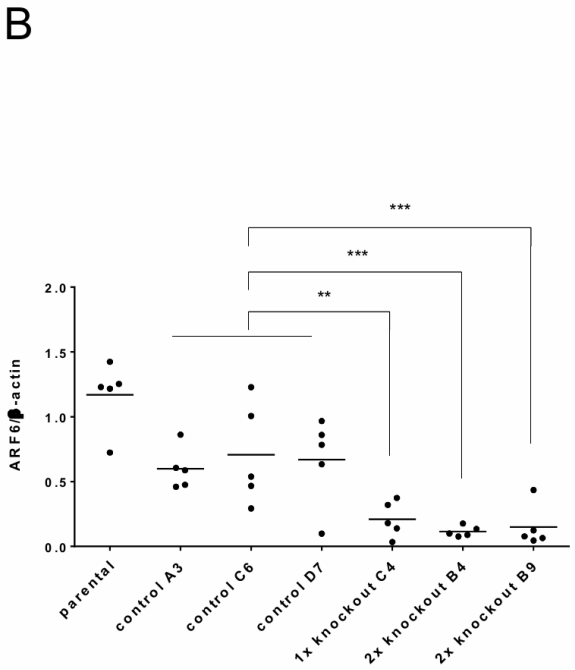

Figure 1

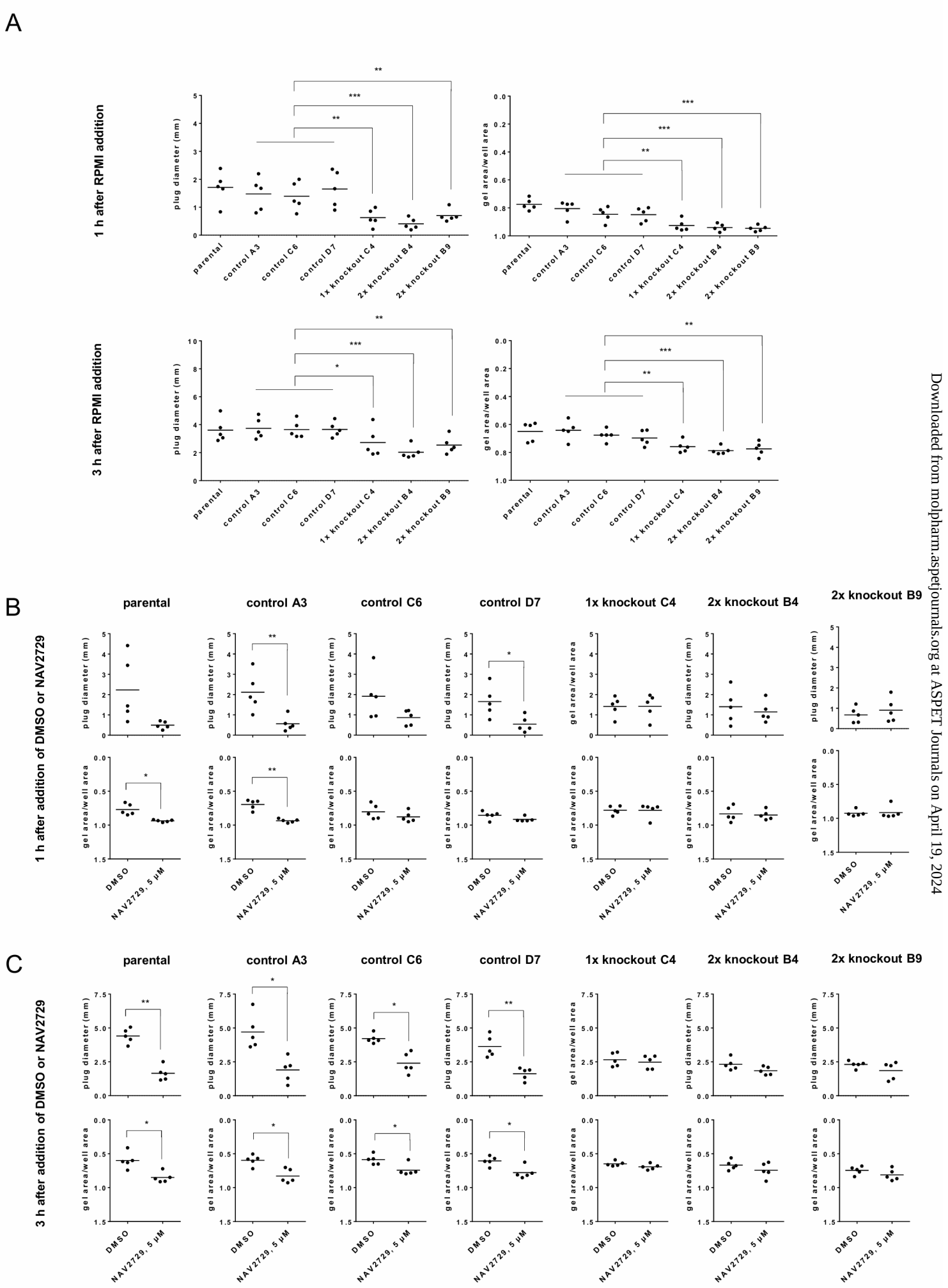

Figure 2

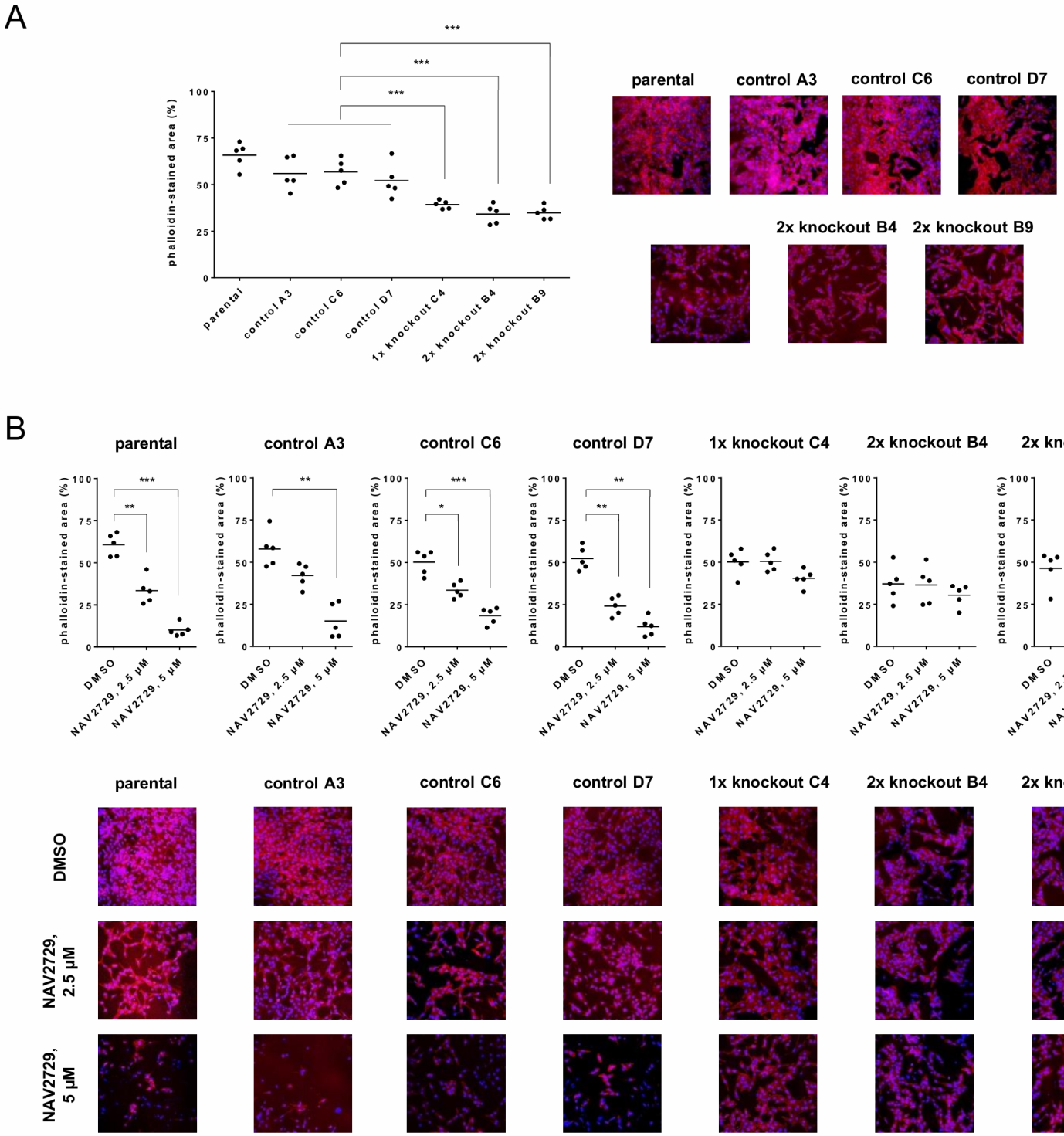

Figure 3

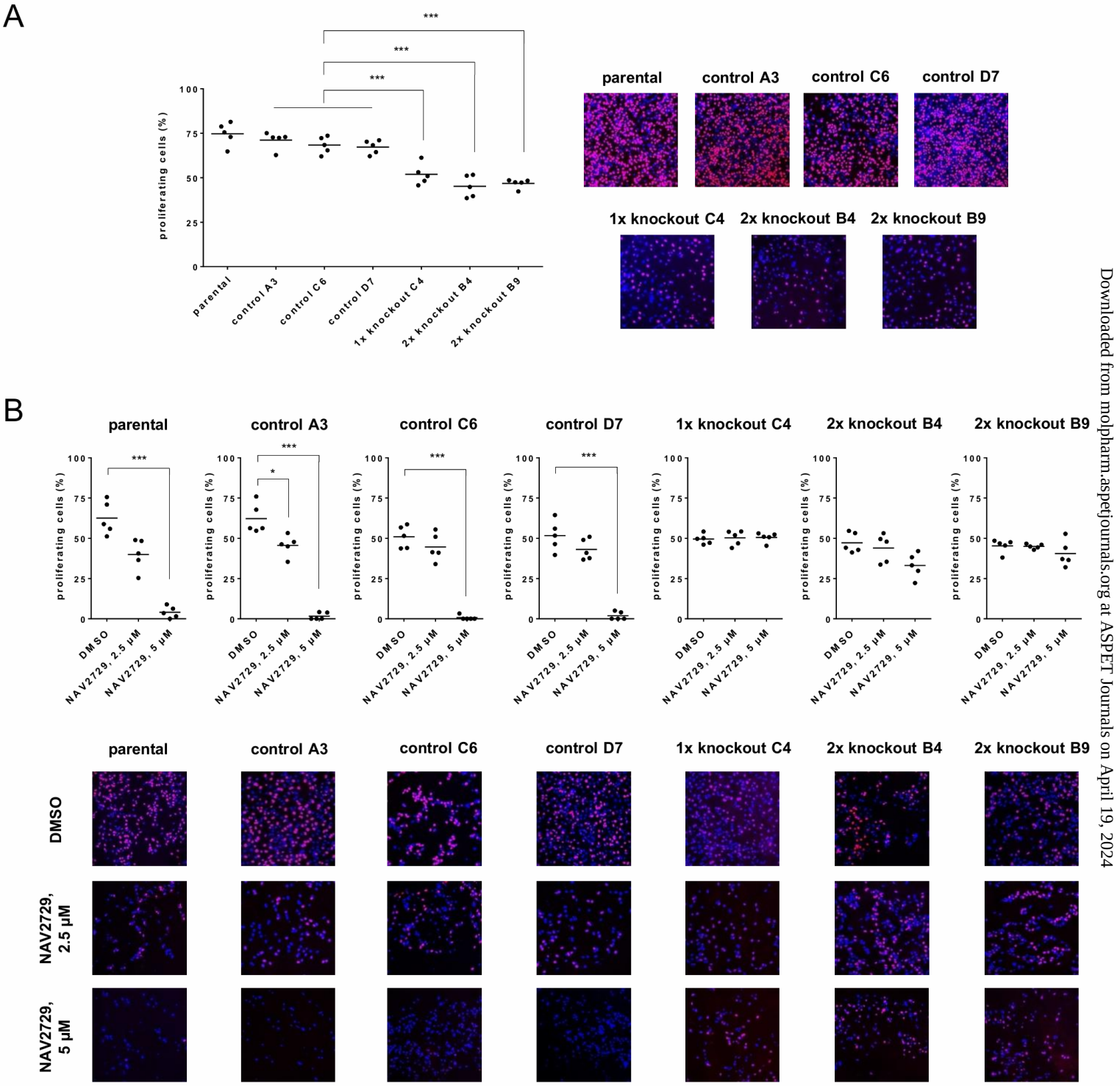

Figure 4

A

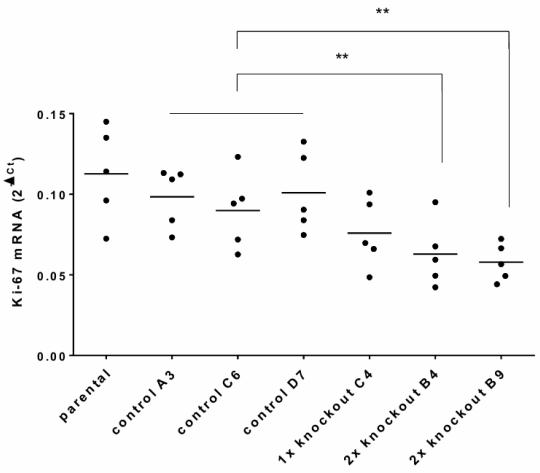

B

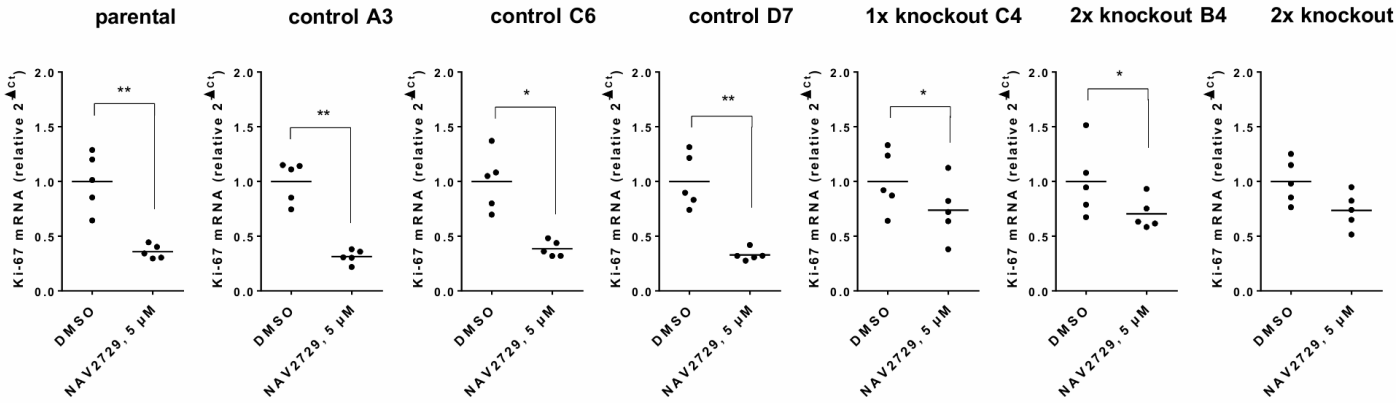

Figure 5

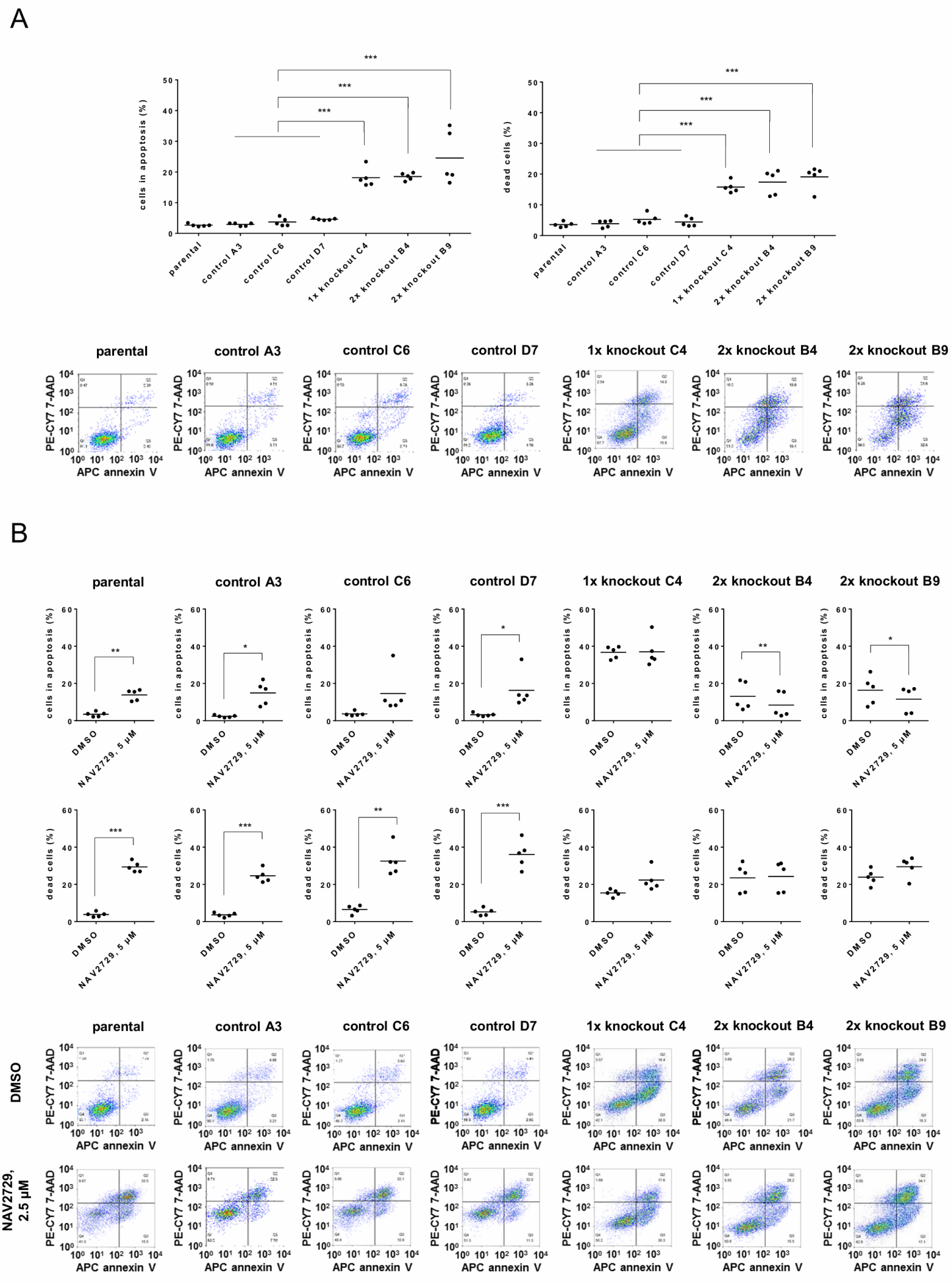

Figure 6

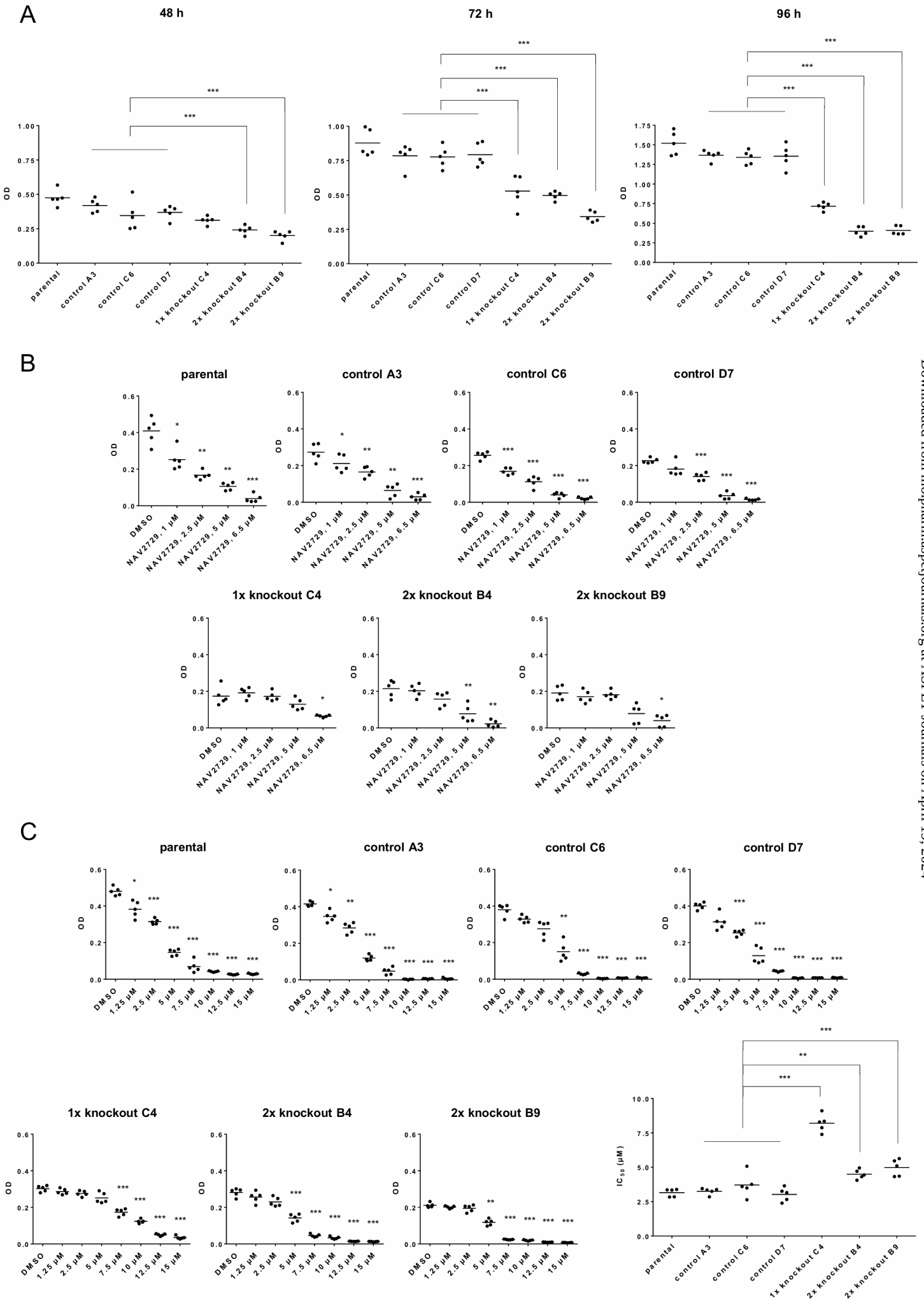

Figure 7